CAPITAL UNIVERSITY OF SCIENCE AND TECHNOLOGY,
ISLAMABAD

Chemical reaction and non-uniform internal heat source effects on the flow of Maxwell nanofluid over a stretching surface

by

Masood Akhtar

A thesis submitted in partial fulfillment for the
degree of Master of Philosophy

in the

Faculty of Computing
Department of Mathematics

October 6, 2017

Declaration of Authorship

I, Masood Akhtar, declare that this thesis titled, 'Chemical reaction and non-uniform internal heat source effects on the flow of Maxwell nanofluid over a stretching surface' and the work presented in it is my own. I confirm that:

- This work was done wholly or mainly while in candidature for a research degree at this University.
- Where any part of this thesis has previously been submitted for a degree or any other qualification at this University or any other institution, this has been clearly stated.
- Where I have consulted the published work of others, this is always clearly attributed.
- Where I have quoted from the work of others, the source is always given. With the exception of such quotations, this thesis is entirely my own work.
- I have acknowledged all main sources of help.
- Where the thesis is based on work done by myself jointly with others, I have made clear exactly what was done by others and what I have contributed myself.

Signed: _____

Date: _____

"The roots of education are bitter but the fruit is sweet."

Aristotle

Abstract

An analysis is made to examine the chemical reaction and non-uniform internal heat and source effects on magneto hydrodynamic mixed convection stagnation point flow of Maxwell nanofluid passing over a stretching surface. The governing partial differential equations are transformed into a system of ordinary differential equations by utilizing similarity transformations. An effective shooting technique of Newton is utilize to solve the obtained ordinary differential equations with the help of software Matlab. The built-in Matlab function bvp4c is also used to strengthen the numerical results. The effects of sundry parameters on the velocity, temperature and concentration distributions are examined and presented in the graphical form. These non-dimensional parameters are the velocity ratio parameter (A), Biot number (Bi), Lewis number (Le), magnetic parameter (M), heat generation/absorption coefficients (A^*, B^*), visco-elastic parameters (β), Prandtl number (Pr), Brownian motion parameter (Nb) and local Grashof number (Gc, Gr).

Acknowledgements

All praises to Almighty **Allah**, the creator of all the creatures in the universe, who has created us in the structure of human beings as the best creature. Many thanks to Him, who created us as a muslim and blessed us with knowledge to differentiate between right and wrong. Many many thanks to Him as he blessed us with the Holy Prophet, **Hazrat Muhammad (Sallallahu Alaihay Wa'alihi wasalam)** for Whom the whole universe is created. He (Sallallahu Alaihay Wa'alihi wasalam) brought us out of darkness and enlightened the way to heaven. I express my heart-felt gratitude to my supervisor **Dr. Muhammad Sagheer** for his passionate interest, superb guidance and inexhaustible inspiration through out this investigation. His textural and verbal criticism enabled me in formatting this manuscript. I would like to acknowledge CUST for providing me such a favourable environment to conduct this research. I especially deem to express my unbound thanks to **Dr. Shafqat Hussain** for his excellent supervision merged with his affection and obligation, without him I would have not been able to commence this current research study.

I would also like to thank especially to the PhD scholar **Mr. Sajid Shah** for his valuable guidance, suggestions and comments in the completion of my thesis. My heartiest and sincere salutations to my Parents, who put their unmatchable efforts in making me a good human being. I also feel grateful to my dearest brothers **Muhammad Azhar, Mansoor Akhtar, Muhammad Farrukh** and my dearest sisters **Kainat Akhtar** and **Inbaisat Akhtar**, who never let me down and always fortified me throughout the hard period of my research work. I also acknowledge my dear friends **Muhammad Bilal, Yasir Mehmood, Khalid Mehmood, Farooq Aslam, Aftab Ahmed, Usman Ali, Umair Farooq,** and **Farrukh Saleem** from the core of my heart for their help, sustenance and effort at lifting me up whenever I was doleful.

May Almighty Allah shower His choicest blessings and prosperity on all those who helped me in any way during the completion of my thesis.

Contents

List of Figures

List of Tables

Abbreviations

ODE	Ordinary differential equation
PDE	Partial differential equation
BVP	Boundary value problem
IVP	Initial value problem
MHD	Magnetohydrodynamics
BC	Boundary condition

Nomenclature

A	velocity ratio parameter,	T	temperature of the fluid
A^*	space dependent heat	T_f	temperature of a hot fluid
	generation/absorption coefficient	T_∞	ambient temperature
$B_\circ$	magnetic field strength	U_∞	free stream velocity
Bi	Biot number	u, v	velocity components
B^*	temperature dependent heat	α	thermal diffusivity
	generation/absorption coefficient	β	visco-elastic parameter
C	concentration at the surface	η	dimensionless similarity variable
C_f	skin friction coefficient	μ	dynamic viscosity of the fluid
C_∞	ambient concentration	υ	kinematic viscosity of the fluid
D_B	Brownian diffusion coefficient	$(\rho)_f$	density of the base fluid
D_T	thermophoresis diffusion coefficient	$(\rho c)_f$	heat capacity of the base fluid
Gc	solutal Grashof number	$(\rho c)_p$	effective heat capacity of
Gr	thermal Grashof number		nanoparticle
Le	Lewis number	Ψ	stream function
M	magnetic parameter	σ	electrical conductivity
Nb	Brownian motion parameter	θ	dimensionless temperature
Nt	thermophoresis	τ_w	wall shear stress
Nu	Local Nusselt number	Γ	parameter defined by $\frac{(\rho c)_p}{(\rho c)_f}$
Pr	Prandtl number	w	condition at the surface
q_w	wall heat flux	γ	chemical reaction parameter
Re_x	local Reynolds number	K_1	chemical reaction coefficient

DEDICATION

I dedicate this sincere effort to my beloved ***Parents*** *and my elegant* ***Teachers*** *whose devotions and contributions to my life are really worthless and whose deep consideration on the part of my academic career, made me consolidate and inspired me as I am upto this grade now.*

Chapter 1

INTRODUCTION

During the past few years, investigating the stagnation point flow of nanofluids has become more popular among the researchers. Nanofluids are formed by the suspension of the nanoparticles in conventional base fluids. Examples of such fluids are water, oil or other liquids. The nanoparticles conventionally made up of carbon nanotubes, carbides, oxides or metals, are used in the nanofluids. Keen interest has been taken by many researchers in the nanofluids as compared to the other fluids because of their significant role in industry, medical field and a number of other useful areas of science and technology. Some prominent applications of these fluids are found in magnetic cell separation, paper production, glass blowing, cooling the electronic devices by the cooling pad during the excessive use, etc. Choi [1] introduced the idea of nanofluids for improving the heat transfer potential of the conventional fluids. He experimentally concluded with an evidence that injection of these particles helps in improving the fluid's thermal conductivity.This conclusion opened the best approach to utilize such fluids in mechanical engineering, chemical engineering, pharmaceuticals and numerous different fields. Buongiorno [2], Kuznetsov and Nield [3] followed him and extended the investigation. They worked on the effects of Brownion motion in convactive transport of nanofluids and the investigation of natural convactive transport of nanofluids passing over a vertical surface in a situation when nanoparticles are dynamically controlled at the boundary. Khan and Pop [4] used this concept to evaluate the laminar boundary layer flow, nanoparticles fraction and heat transfer for nanofluids passing over a stretching surface. Zheng et al. [5] explored the effects of rediation on the flow and heat transfer of

nanofluids past a stretched surface with temperature jump and velocity slip in a porous media.

Impact of radiation upon the heat and mass transfer of the fluids is of remarkable consideration at high operating temperature. In the field of engineering, many procedures are executed at high temperature. In such situations, the analysis of the radiation heat transfer plays a key role for the selection of an appropriate equipment. Examples of such fields are atomic and nuclear power plants, artificial satellites, the gas turbines, aircraft industry, missiles manufacturing and wind-turbines etc. Takhar et al. [6] examined the impact of radiation on the magnetohydrodynamic free convection spill for non-gray gas over a semi-infinite plumb surface. Ghaly and Elbarbary [7] delineated the consequences of radiation on the free convection flow of a gas under the MHD effect across a stretching surface with uniform free stream. Devi and Kayalvizhi [8] delivered the analytical solution of MHD flow with radiation passing over a stretching sheet in a porous medium.

In industrial sector and modern technology, the non-Newtonian fluids play a vital role. Non-Newtonian fluids have some interesting applications as they are used in the manufacturing of sports shoes, flexible military suits and viscous coupling. Rising inception of the non-Newtonian fluids like emulsions, molten plastic pulp, petrol and many other chemicals has triggered an appreciable interest in the study of the behavior of such fluids during motion. The mathematical solutions of the models involving the non-Newtonian fluids, are quite interesting and physically applicable. Makinde [9] investigated the buoyancy effect on magnetohydrodynamic stagnation point flow and heat transfer of nanofluids passing over a convectively heated stretching/shrinking sheet. The MHD flow characteristics of a visco-elastic fluid passing over a stretched surface, were studied by Andersson [10]. Later, this work was extended by M. I. Char [11] by including an analysis of the mass transfer. Second order incompressible fluid flows were examined by Marcovitz and Coleman [12]. Rajagopal [13] investigated the unsteady and undirectional flow of a non-Newtonian fluid. Later, Rajagopal and Gupta [14] presented an exact solution of a mathematical model describing the flow of non-Newtonian fluid passing over a porous infinite plate. Siddique et al [15] employed the hodograph transformation technique for the mathematical investigation of the flow of non-Newtonian fluid. Some inverse solutions of the non-Newtonian fluid models were worked out by Siddiqui and Kaloni [16]. Chandna and Nguyen [17] used the hodograph transformation technique to get the solution of the non-Newtonian MHD transverse fluid flow problems.

Non-Newtonian fluids flows with MHD effects across the orthogonal steady plane were examined by Nguyen and Chandna [18]. The MHD fluid passing over a stretched sheet, through the porous media with the thermal radiation and the thermal conductivity was examined by Cortell [19]. A few recent contributions regarding flow of Non-Newtonian fluid models can be seen in [20–44].

Krishna et al. [45] explored the 2-D stagnation flow of viscous incompressible fluids in the presence of thermal radiation, internal heat generation and chemical reaction over a stretched surface. The heat and mass transfer analysis of MHD free convective incompressible fluid over a vertical stretched surface in the presence of chemical reaction through a porous media, was explored by Mansour et al. [46]. Naramgari and Sulochana [47] outlined the mass and heat transfer of the thermophoretic fluid flow past an exponentially stretched surface inserted in porous media in the presence of internal heat generation/absorption, infusion and viscous dissemination. Afify [48] examined the MHD free convective heat and fluid flow passing over the stretched surface with chemical reaction. A numerical analysis of insecure MHD boundary layer flow of a nanofluid past an stretched surface in a porous media was carried out by Anwar et al. [49]. Nadeem and Haq [50] studied the magnetohydrodynamic boundary layer flow with the effect of thermal radiation over a stretching surface with the convective boundary conditions.

Thesis Contribution:

In this thesis, we first reproduce an analysis study of [51] and then extend the "MHD stagnation point flow of nanofluid past a stretching sheet with convective boundary condition." According to our information, "chemical reaction and non-uniform internal heat source effects on MHD mixed convection stagnation point flow of Maxwell nanofluid over a stretching surface" is not yet examined. An appropriate similarity transformation has been utilized to acquire the system of nonlinear and coupled ODEs from the system of PDEs. Results are acquired numerically by using the comprehensive shooting scheme and also compared with those obtained through the MATLAB bvp4c code to strengthen the solution. The numerical results are analyzed by graphs for different parameters which appear in the solution affecting the MHD mixed convection stagnation point.

Draft Of Thesis:

The thesis is categorized as the following order;

In **Chapter 2**, there are some basic definitions of fluid, fluid mechanics, hydrostatics, hydrodynamics, heat transfer, boundary layer flow and basic governing laws have been presented. These basic concepts are used further in describing the flow, heat transfer, stagnation point and the influence of magnetohydrodynamic on Maxwell nanofluids.

Chapter 3 contains a detailed review of [51]. A study of the flow of nanofluid passing over a stretched surface with the MHD stagnation point and the convactive boundary condition has been analyzed numerically. The numerical solution of governing equations is obtained and impact of parameters regarding skin-friction coefficient and local Nusselt number are shown through tables and graphs. Also an perfect match of our numerical result is found with those of the previously published results of Ibrahim and Haq [51].

In **Chapter 4**, we explore the aspects of chemical reaction and non-uniform internal heat and source effects on MHD mixed convaction stagnation point flow of Maxwell nanofluid passing over a stretched surface. The obtained system of ordinary differential equations by applying the useful similarity transform are solved numerically. Behavior of physical parameters has been presented in tabular form and through graphs. In this thesis, we also compute and discuss the numerical values of skin-friction coefficient and local Nusselt number.

In **Chapter 5**, we recapitulate the treatise and give the conclusion occurring from the entire research and opening of the future work.

All the references used in this treatise are listed in **Bibliography**.

Chapter 2

LITERATURE REVIEW

In current Chapter, some definitions, basic laws, terminologies, basic concepts and some classical methods for solving nonlinear differential equations would be described (see Thermodynamics [52]), which would be used in next chapters.

2.1 Preliminaries

Definition 2.1.1. (Fluid) "A fluid is a substance that continuously deforms under an applied shear stress. Fluid has no proper shape and continuously deforms until a shear stress of any magnitude acts upon it. This shear stress may be less or more through which fluid changes its shape." The study of fluids is divided into two categories:

- Newtonian fluids
- Non-Newtonian fluids

Definition 2.1.2. (Newtonian Fluid) "Fluids which obey the Newton's law of viscosity are called Newtonian fluids. Newton's law of viscosity states that the shear stress between adjacent fluid layers is proportional to the negative value of velocity gradient between two layers."

Definition 2.1.3. (Non-Newtonian Fluid) "Fluids which do not obey the Newton's law of viscosity are called the non-Newtonian fluids."

Definition 2.1.4. (Fluid Mechanics) "Fluid mechanics deals with the study of all fluids under static and dynamic conditions. Fluid mechanics is the branch which deals with a relationship between motion, force and statical conditions."

Definition 2.1.5. (Hydrostatics) It is the branch of fluid mechanics which deals with the study of incompressible fluids at rest. It surrounds the study of the conditions under which fluids are at rest in stable equilibrium. It is opposite in nature to fluid dynamics, the study of fluids in motion. Hydrostatics are classified as a part of the fluid statics, which is the study of all fluids at rest whether incompressible or not.

Definition 2.1.6. (Fluid Dynamics) It is the study of the motion of liquids, gases and plasmas from one place to another. Fluid dynamics has a wide range of applications like calculating force and moments on aircraft, mass flow rate of petroleum passing through pipelines, prediction of weather, etc.

Definition 2.1.7. (Hydrodynamics) The study of liquids in motion is called hydrodynamics.

Definition 2.1.8. (Conservation Laws) There are three conservation laws which are used to model the problems of fluid dynamics, and may be written in integral or differential form. Integral formulations of these laws consider the change of mass, momentum or energy within the control volume or fixed region.

Definition 2.1.9. (Conservation of Mass) "The rate of change of mass inside a control volume must be equal to the net rate of fluid flow into the volume. Physically, this statement requires that mass is neither created nor destroyed in the control volume, and can be translated into the differential form of the continuity equation.

$$\frac{\partial \rho}{\partial t} + \nabla.(\rho \mathbf{V}) = 0. \tag{2.1}$$

If the density is constant and spatially uniform, in that case Eq. (2.1) becomes

$$\nabla \cdot \mathbf{V} = 0.$$

In this case density is constant."

Definition 2.1.10. (Conservation of Momentum) "It stats that the total linear momentum of a closed system remains constant, regardless of other possible changes

within the closed system. The differential form of momentum conservation equation is as follow;"

$$\frac{D\mathbf{u}}{Dt} = \mathbf{F} - \frac{\nabla \mathbf{p}}{\rho}.$$

Definition 2.1.11. (Conservation of Energy) "The total energy in a given closed system remains constant and it is neither created nor destroyed, although it can be converted from one form to another.

$$\rho \frac{D\mathbf{h}}{Dt} = \frac{D\mathbf{p}}{Dt} + \nabla.(\kappa \nabla T) + \phi$$

In the above equation, $\mathbf{h}$ is enthalpy, k is thermal conductivity of fluid, T denotes temperature and ϕ is viscous dissipation function. The viscous dissipation function controls the rate at which mechanical energy is converted into heat energy. The expression on left hand side is material derivative."

Definition 2.1.12. (Compressible and Incompressible Flows) Compressible flow is the branch of fluid mechanics which deals that flows having significant changes in density of fluid. Mostly, gases display such behaviour. Density may change due to the changes in pressure or temperature. However, in many cases the changes in temperature and pressure are so small that these can be neglected. In this situation, the flow is modelled as an incompressible flow. Otherwise the more general compressible flow equation is used. Mathematical form of incompressibility is expressed as

$$\frac{D\rho}{Dt} = 0,$$

where ρ denotes the fluid density and $\frac{D}{Dt}$ is the substantial derivative which is given by sum of local and convective derivative in the form;

$$\frac{D}{Dt} = \frac{\partial}{\partial t} + \mathbf{V} \cdot \nabla. \tag{2.2}$$

In Eq. (2.2), $\mathbf{V}$ denotes the velocity of the flow and ∇ is the differential operator.

Definition 2.1.13. (Uniform and Non-uniform Flows) When velocity and other hydrodynamic parameters remain the same from point to point at any instant of time, then it is called uniform flow. But if velocity changes from point to point at given instant of time, then the flow is called non-uniform flow.

Definition 2.1.14. (Stationary and Non-stationary Flows) If the flow is such that the velocity, pressure and other properties at every point in the flow do not depend upon time, it is called stationary or steady flow, i.e.,

$$\frac{\partial \lambda}{\partial t} = 0,$$

where λ is any fluid property.
Non-stationary flow is one where the physical properties do depend on time, i.e.,

$$\frac{\partial \lambda}{\partial t} \neq 0.$$

Definition 2.1.15. (Streamline and Turbulent Flows) "When a fluid flows in parallel layers, without disruption (disturbance) between the layers, it is called streamline or laminar flow. It is the flow of a fluid when each particle of the fluid follows a smooth pattern, the pattern which never interfere with one another. In streamline flow, the velocity of the fluid is constant at any point in the fluid. In contrast the turbulent flow is the flow in which fluid undergoes irregular fluctuations. In turbulent flow, speed of fluid at a point continuously changes in both magnitude and direction."

Definition 2.1.16. (Viscosity) "The viscosity of a fluid is demarcate of its resistance to moderate deformation by shear stress or tensile stress. For liquids, it corresponds to the real concept of thickness, for example, honey has much higher viscosity than water. Viscosity is the property of a fluid that resists the relative motion in between the two layers of fluid that are moving with different velocities. A fluid that has zero viscosity is called ideal od inviscid fluid. Zero viscosity is observed only at very low temperature in superfluids." Viscosity is denoted by μ. There are two common kinds of viscosity namely the kinematic and dynamic.

Definition 2.1.17. (Absolute Viscosity) Measurement of the fluid's internal resistance to flow is called absolute or dynamic viscosity. This resistance appears by the forces of attraction between the molecules of the fluid.
Mathematically, it can be written as the ratio between shear stress and the rate of shear strain.

$$\text{Viscosity}(\mu) = \frac{\text{Shear stress}}{\text{Rate of shear strain}}.$$

In the above expression μ is called the coefficient of viscosity which has dimension $[ML^{-1}T^{-1}]$. Unit of viscosity in SI system is kg/ms or Pascal-second.

Definition 2.1.18. (Kinematic Viscosity) Kinematic viscosity is the ratio of absolute or dynamic viscosity μ to density ρ. It is denoted by ν.
Mathematically it can be written as,

$$\nu = \frac{\mu}{\rho},$$

It has a dimension $[L^2T^{-1}]$ and its unit in SI system is meter square per second.

- "For a liquid, the kinematic viscosity decreases with higher temperature."
- "For a gas, the kinematic viscosity increases with higher temperature."

Definition 2.1.19. (Nanofluid) A nanofluid is that fluid which contains particles having size of nanometer. The nanoparticles used in nanofluids are usually made of metals, carbides, oxides or carbon nanotubes.

Definition 2.1.20. (Stagnation Point) In fluid dynamics, stagnation point is that point in a flow field where local velocity of the fluid becomes zero.

Definition 2.1.21. (Stagnation Pressure) Stagnation pressure or pitot pressure is the static pressure at stagnation point in a fluid flow. At a stagnation point, the velocity of fluid becomes zero and all kinetic energy is turned into pressure energy.

Definition 2.1.22. (Magnetohydrodynamics) Magnetohydrodynamics (magneto fluid dynamics or hydromagnetics) is the branch that studies the magnetic properties of electrically conducting fluids. Examples of such magneto fluids include plasmas, molten metals and salt water or electrolytes.

Definition 2.1.23. (Heat Transfer) Heat is transfered from hot medium to the cold medium. Heat transfer ceases when thermal equilibrium is reached. There are three fundamental modes of transfer of heat, which are conduction, convection and radiation.

Definition 2.1.24. (Conduction) Conduction is a process by which the heat energy is transmitted through collisions between neighboring molecules. In other words, conduction is the way through which energy is transferred by the movement of electrons or ions.

Definition 2.1.25. (Convection) Convection is the transfer of heat energy into or out of the body by actual movement of fluids particles that transfer energy with its mass. Initially heat is transferred by conduction between the object and fluid, the bulk transfer of energy comes from motion of the fluid. Convection may arise in three different forms which are spontaneous or natural or free convection, the forced and mixed convection. Here are some examples of convection.

- "Boiling water - The heat passes from the burner into the pot, heating the water at the bottom. Then, this hot water rises and cooler water moves down to replace it, causing a circular motion."
- "Radiator - Puts warm air out at the top and draws in cooler air at the bottom."
- "Ice melting - Heat moves to the ice from the air. This causes the melting from solid to liquid."
- "Hot air balloon - A heater inside the balloon heats the air and so the air moves upward. This causes the balloon to rise because the hot air gets trapped inside. When the pilot wants to descend, he releases some of the hot air and cool air takes it place which causes the balloon to move down."

Definition 2.1.26. (Spontaneous Convection) Spontaneous convection occurs when there is no wind or other stream of fluid past the body. Instead, the fluid in contact with the object moves away in a less predictable manner. Due to thermal convection current, it expands and floats on surface because it is less densed than the other fluids surrounding it. It is more usually called free convection.

Definition 2.1.27. (Forced Convection) It is a mechanism or method of transport in which fluid motion is generated by the external source (like fan, pupm or suction devices etc.). It is considered as one of the important methods of useful heat transfer as significant amount of heat energy can be transported in very efficient way.

Definition 2.1.28. (Combined Convection) Combined or mixed convection is the combination of spontaneous and forced convection which is the general case of convection when a flow is determined simultaneously by both outer force system (i.e., outer energy supply to the fluid streamlined body system) and volumetric (mass) force , viz., by the

nonuniform density distribution of a fluid medium in a gravity field. In other words, when both natural and forced convection processes simultaneously and significantly contribute to heat transfer, mixed convection flow appears.

Definition 2.1.29. (Radiation) Transfer of heat due to emission of electromagnetic waves is called the radiation or thermal radiation. Heat transfer by radiation takes place in the form of electromagnetic waves mainly in infrared region. A body emits radiation which is the result of thermal agitation of its composing molecules.

Definition 2.1.30. (Thermal Diffusivity) Thermal diffusivity is material-specific property for characterizing unsteady heat conduction. Through this value, it is measured that how quickly a body changes its temperature. In order to predict cooling process or to stimulate temperature field, thermal diffusivity must be known. Mathematically, it can be expressed as

$$\alpha = \frac{\kappa}{\rho C_p},$$

where κ, ρ and C_p represent the thermal conductivity of material, the density and the specific heat capacity. The unit and dimension of thermal diffusivity in SI system are $m^2 s^{-1}$ and $[LT^{-1}]$ respectively.

Definition 2.1.31. (Thermal Conductivity) Thermal conductivity (κ) is the property of a material to conduct heat. Mathematically it can be written as,

$$\kappa = \frac{q\nabla l}{S\nabla T},$$

where q is the heat passing through a surface area denoted by S which causes difference in temperature ∇T over a distance of ∇l. Here l, S and ∇T all are supposed to be of unit measurement. In SI system the unit of thermal conductivity is $\frac{W}{m.\kappa}$ and its dimension is $[MLT^{-3}\theta^{-1}]$.

2.2 Dimensionless Parameters

Definition 2.2.1. (Biot Number (Bi)) It is a dimensionless number used in the calculation of heat transfer. It is named due to a French physicist Jean-Baptiste Biot and gives simple index of ratio of resistance of heat transfer inside and at the surface of

body. Mathematically,

$$Bi = \frac{h_f}{k}.(\frac{\nu}{a})^{\frac{1}{2}},$$

where h is the convective heat transfer coefficient or heat transfer coefficient.

Definition 2.2.2. (Skin-friction Coefficient (C_f)**)** It occurs in between the solid and fluid surface through which motion of fluid becomes slow. It is proportionality between the shearing stress exerted by the fluids at the earth's surface and the square of the surface fluids speed. The skin friction coefficient can be defined as,

$$C_f = \frac{2\tau_w}{\rho U^2},$$

where τ_w represents the wall shear stress, ρ denotes the density and U is the free-stream velocity.

Definition 2.2.3. (Reynolds Number (Re)**)** It is the most considerable dimensionless number which is used to discern the different flow behaviors such as laminar or turbulent flow. It helps to measure the ratio of inertial force to the viscous force. Mathematically,

$$Re = \frac{\frac{\rho U^2}{L}}{\frac{\mu U}{L^2}} \quad \Longrightarrow \quad Re = \frac{LU}{\nu},$$

where U represents the free stream velocity, L denotes the characteristics length and ν stands for kinematic viscosity. At low Reynolds number, laminar flow arises, where viscous forces are governing. At high Reynolds number, turbulent flow appears, where the inertial forces are governing.

Definition 2.2.4. (Lewis Number (Le)**)** It is a dimensionless number defined as the ratio between thermal diffusivity and mass diffusivity. It is used to characterize the fluid flow where simultaneous heat and mass transfer exist. Mathematically,

$$Le = \frac{\alpha}{D_B},$$

where α is the thermal diffusivity and D_B is the mass diffusivity. Lewis number can also be written in the form of Prandtl number and the Schmidt number as

$$Le = \frac{Sc}{Pr}.$$

Definition 2.2.5. (Prandtl Number (Pr)**)** This number is dimensionless. It is the ratio of the momentum diffusivity (ν) to thermal diffusivity (α). Mathematically,

$$Pr = \frac{\nu}{\alpha} \quad \Longrightarrow \quad \frac{\mu/\rho}{k/c_p} \quad \Longrightarrow \quad \frac{\mu c_p}{k},$$

where μ stands for the dynamic viscosity, C_p denotes the specific heat and κ represents the thermal conductivity. The relative thickness of thermal boundary layer and momentum boundary layer are controlled by this number.

Definition 2.2.6. (Nusselt Number (Nu)**)** At the surface within the fluid, the nusselt number (Nu) is the ratio of convective to conductive heat transfer normal to the surface.

$$Nu = \frac{hL}{\kappa},$$

where h stands for convective heat transfer, L represents the characteristics length and κ denotes the thermal conductivity.

Definition 2.2.7. (Grashof Number (Gr) It is a dimensionless number in fluid dynamics and heat transfer which approximates the ratio between buoyancy force and viscous force acting on fluid. It frequently arises in the study of situations involving natural convection. Mathematically it can be written as,

$$Gr = g\frac{\beta_T}{a^2 x}(T_f - T_\infty),$$

$$Gc = g\frac{\beta_C}{a^2 x}C_\infty.$$

2.3 Boundary Layer Flow

A thin layer of a flowing gas or liquid in contact with some body like wings of airplane or interior of a pipe. In the boundary layer the fluid is subjected to the shearing forces. The fundamental idea of boundary layer in motion of fluid passing over a surface was first presented by Ludwig Prandtl (1874-1953). The reason why we have the zero velocity precisely besides the layer is that the adherent effect and the layer of fluid which is making association with surface becomes slowly adhered to the surface, resulting in a condition of no-slip. The experience of shearing occurs in the process due to the fact that the layers of fluid are moving. The shear acting between the two walls and the

layer just next is called wall shear and it is denoted by T_w. Boundary layer has two following types:

- Hydrodynamic (velocity) boundary layer
- Thermal boundary layer

Definition 2.3.1. (Hydrodynamic Boundary Layer) "It is a region of a fluid near to the solid surface where the flow patterns are directly affected by the viscous pull from the surface wall."

Definition 2.3.2. (Thermal Boundary Layer) "It is the layer of a gaseous or liquid heat-transfer agent between the free stream and a heat-exchange surface. In this layer the temperature of the heat-transfer agent changes from that of the wall to that of the free stream."

Chapter 3

MHD STAGNATION POINT FLOW OF NANOFLUID PAST A STRETCHING SHEET

3.1 Introduction

In this chapter, we provide the detailed review of [51]. The numerical results in [51], were aquired by using bvp4c, a Matlab built-in code. In this chapter, we reproduce the same results by bvp4c and additionally by the shooting method. In literature, zero normal flux condition of the nanoparticles is the recent phenomenon which has not seem to be investigated at the wall for the flow. The nanoparticle fractions are supposed to be inactively controlled on the boundary. The system of governing non-linear PDEs is converted into the nonlinear ODEs by using the appropriate similarity transformation. A renowned shooting technique is used to solve the obtained equations numerically for estimations of different physical parameters. Results are achieved numerically for concentration, temperature, velocity, local Nusselt number and for the skin friction coefficient. These results are found to be in a very decent concurrence with those obtained by the bvp4c.

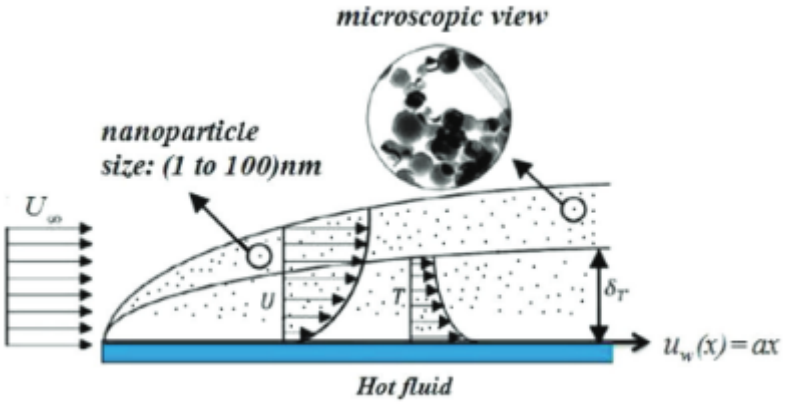

FIGURE 3.1: Geometry for the flow under consideration.

3.2 Mathematical Modeling

Consider the stagnation point flow of two dimensional viscous steady flow of nanofluid passing over a stretched surface with the convective BC. The stretching sheet was heated with the temperature T_f and the heat transfer coefficient h_f at its lower surface. Here, concentration and uniform ambient temperature are respectively C_∞ and T_∞.

"Assume that at the surface, there is not any nanoparticle flux and the impacts of the thermophoresis is taken as a BC. In flow model, $u_w(x) = ax$ is the velocity of the stretching surface, where "a" is any constant. In the direction of the flow, normal to the surface, it is directed towards the magnetic field of strength B_o which is supposed to be applied in the direction of +ve $y-$axis. Here magnetic field is negligible because of assumption of very small when comparing with the applied magnetic field. The preferred system of coordinates is such as $x-$axis is directed to the flow and $y-$axis is perpendicular to it. Proposed coordinate system and flow model are presented in Figure 3.1.

Flow model of [51] shows that In the presence of magnetic field over the surface, the governing equations of conservation of momentum, energy, mass and nanoparticle fraction, under the boundary layer approximation, are as follows:

$$\frac{\partial u}{\partial x}+\frac{\partial v}{\partial y}=0, \tag{3.1}$$

$$u\frac{\partial u}{\partial x}+v\frac{\partial u}{\partial y}=v\frac{\partial^2 u}{\partial y^2}+U_\infty\frac{\partial U_\infty}{\partial x}+\frac{\sigma B_o^2}{\rho_f}(U_\infty-u), \tag{3.2}$$

$$u\frac{\partial T}{\partial x}+v\frac{\partial T}{\partial y}=\alpha\frac{\partial^2 T}{\partial y^2}+\Gamma\left[D_B\left(\frac{\partial C}{\partial y}\frac{\partial T}{\partial y}\right)+\frac{D_T}{T_\infty}\left(\frac{\partial T}{\partial y}\right)^2\right], \tag{3.3}$$

$$u\frac{\partial C}{\partial x}+v\frac{\partial C}{\partial y}=D_B\frac{\partial^2 C}{\partial y^2}+\frac{D_T}{T_\infty}\left(\frac{\partial^2 T}{\partial y^2}\right). \tag{3.4}$$

The associated boundary conditions are:

$$\left.\begin{aligned} &u=u_w=ax,\ v=0,\ -k\frac{\partial T}{\partial y}=h_f(T_f-T),\ D_B\frac{\partial C}{\partial y}+\frac{D_B}{T_\infty}.\frac{\partial T}{\partial y}=0 \text{ at } y=0,\\ &u\to U_\infty=bx,\ v=0,\ T\to T_\infty\ C\to C_\infty \text{ as } y\to\infty, \end{aligned}\right\} \tag{3.5}$$

where x is the coordinate axis along the continuous surface in the direction of motion and y is the coordinate axis along the continuous surface in the direction perpendicular to the motion. The components of velocity along $x-$ and $y-$ axis are respectively u and v. Here kinematics velocity is represented by υ and T represents the temperature inside the boundary layer. The parameter Γ is defined by $\Gamma=\frac{(\rho c)_p}{(\rho c)_f}$, where $(\rho c)_p$ is effective heat capacity of nanoparticles and $(\rho c)_f$ is heat capacity of base fluid, ρ is the density and T_∞ is the ambient temperature faraway from the surface.

3.3 Dimensionless Form of the Model

To convert the PDEs (3.1)-(3.4) along with the BCs (3.5) into the dimensionless form, we use the following similarity transformation;

$$\eta=\sqrt{\frac{a}{\upsilon}}y,\ \psi=\sqrt{a\upsilon}xf(\eta),\ \theta(\eta)=\frac{T-T_\infty}{T_f-T_\infty},\ \phi(\eta)=\frac{C-C_\infty}{C_\infty}, \tag{3.6}$$

where $\psi(x,y)$ denotes stream function given by

$$u=\frac{\partial\psi}{\partial y},\qquad v=-\frac{\partial\psi}{\partial x}. \tag{3.7}$$

In Eq. (3.1) is satisfied identically. Remaining governing Eqs. (3.2)-(3.4) are reduced into the nonlinear ODEs by using (3.6), as

$$f''' + ff'' - f'^2 + A^2 + M(A - f') = 0, \tag{3.8}$$

$$\theta'' + Pr(f\theta' + Nb\phi'\theta' + Nt\theta'^2) = 0, \tag{3.9}$$

$$\phi'' + LePrf\phi' + \frac{Nt}{Nb}\theta'' = 0. \tag{3.10}$$

The BCs get the form,

$$f(0) = 0,\ f'(0) = 1,\ \theta'(0) = Bi(\theta(0) - 1),\ Nb\phi'(0) + Nt\theta'(0) = 0,\ \text{at } \eta = 0, \tag{3.11}$$

$$f'(\infty) \to A,\ \theta(\infty) \to 0,\ \phi(\infty) \to 0,\ \text{as } \eta \to \infty. \tag{3.12}$$

The governing parameters are defined as

$$\left.\begin{aligned} Bi = \frac{h_f}{k}\sqrt{\frac{\upsilon}{a}},\ Pr = \frac{\upsilon}{\alpha},\ A = \frac{b}{a},\ Le = \frac{\alpha}{D_B},\ M = \sigma\frac{{B_o}^2}{\rho_f a}, \\ Nb = \frac{(\rho c)_p D_B C_\infty}{(\rho c)_f \upsilon},\ Nt = \frac{(\rho c)_p D_T (T_f - T_\infty)}{(\rho c)_f \upsilon T_\infty}. \end{aligned}\right\} \tag{3.13}$$

In this problem, the desired physical quantities are the skin-friction coefficient C_f and the Nusselt number Nu_x. These quantities are defined as

$$C_f = \frac{\tau}{\rho {u_w}^2},\ Nu_x = \frac{xq_w}{k(T_f - T_\infty)}. \tag{3.14}$$

Here wall heat flux q_w, and wall shear stress τ_w, are given as

$$\tau_w = \mu\left(\frac{\partial u}{\partial y}\right)_{y=0},\ q_w = -k\left(\frac{\partial T}{\partial y}\right)_{y=0}. \tag{3.15}$$

By using the above equations, we have

$$C_f\sqrt{Re_x} = -f''(0),\ \frac{Nu_x}{\sqrt{Re_x}} = -\theta'(0). \tag{3.16}$$

Here $Re_x = \frac{ax^2}{\upsilon}$ is representing the Reynolds number whereas Nu_x is representing the Nusselt number."

3.4 Numerical Results

In this Section, first of all, the scheme for the numerical solution of the system of three coupled ODEs (3.8)-(3.10) with the BCs (3.11)-(3.12) will be discussed. Then, the numerical results in the tabular form will be presented and analyzed. Because of its effeciency, the shooting technique has been prefered to apply. First, the system of equations (3.8)-(3.10) will be transmuted into a system of ODEs. We can write

$$f''' = -ff'' + f'^2 - A^2 - M(A - f'), \tag{3.17}$$

$$\theta'' = -Pr(f\theta' + Nb\phi'\theta' + Nt\theta'^2), \tag{3.18}$$

$$\phi'' = -LePrf\phi' - \frac{Nt}{Nb}\theta''. \tag{3.19}$$

By using the following notations

$$f = y_1,\ f' = y_2,\ f'' = y_3,\ \theta = y_4,\ \theta' = y_5,\ \phi = y_6,\ \phi' = y_7, \tag{3.20}$$

the above system of coupled nonlinear ODEs is transmuted into the following system of seven first order equations:

$$\begin{aligned}
y_1' &= y_2,\\
y_2' &= y_3,\\
y_3' &= y_2^2 - y_1y_3 - A^2 - M(A - y_2),\\
y_4' &= y_5,\\
y_5' &= -Pr(y_1y_5 + Nby_5y_7 + Nty_5^2),\\
y_6' &= y_7,\\
y_7' &= -LePry_1y_7 + Pr\frac{Nt}{Nb}(y_1y_5 + Nby_5y_7 + Nty_5^2).
\end{aligned}$$

The resulting form of the BCs is

$$\begin{aligned}
&y_1(0) = 0,\ y_2(0) = 1,\ y_5(0) = Bi(y_4(0) - 1),\ y_7(0) = -\frac{Nt}{Nb}y_5(0),\\
&y_2 \to A,\ y_4 \to 0,\ y_6 \to 0 \text{ as } \eta \to \infty.
\end{aligned}$$

To execute the numerical procedure, the unbounded domain $[0, \infty)$ has been replaced by $[0, \eta_{max}]$ for some suitable choice of η_{max}. An asymptotic convergence of the numerical

solution is noticed by enlarging the value of η_{max}. The shooting method requires some initial guess for $y_3(\eta)$, $y_4(\eta)$ and $y_6(\eta)$ at $\eta = 0$. The initial guess is updated by the Newton's method until a solution of the problem which approximately meets the given boundary conditions at the right end of the domain.

To validate the numerical results obtained by shooting method, a Matlab built-in function bvp4c is also applied. In Table 3.1, by taking $M = 0$ and update the velocity ratio parameter A, numerical results of the skin-friction coefficient $f'(0)$ are reproduced. It shows a very decent concurrence with those published by Mahpatra and Guppta [53] and Ishak et al [54].

A	Ibrahim [55]	Ishak[54]	Ibrahim [51]	Present	
				Shooting	bvp4c
0.1	-0.9694	-0.9694	-0.9694	-0.9694	-0.9694
0.2	-0.9181	-0.9181	-0.9181	-0.9181	-0.9181
0.3	-	-	-0.8494	-0.8494	-0.8494
0.4	-	-	-0.7653	-0.7653	-0.7653
0.5	-0.6673	-0.6673	-0.6673	-0.6672	-0.6673
0.8	-	-	-0.2994	-0.2993	-0.2994
1.0	-	-	0.0000	0.0000	0.0000
2.0	2.0175	2.0175	2.0175	2.0175	2.0175
3.0	4.7293	4.7293	4.7293	4.7292	4.7293
5.0	-	-	11.7520	11.7519	11.7520
7.0	-	-	20.4979	20.4978	20.4979
10.0	-	-	36.2574	36.2574	36.2574

TABLE 3.1: Comparison of the skin-friction coefficient f'' for different values of velocity ratio parameter A and $M = 0$.

To further investigate the numerical technique used, we ignore the impacts of thermophoresis parameter Nt and Brownian motion parameter Nb and then compare the local Nusselt number $\theta'(0)$ by updating the Prandtl number as shown in Table 3.2. Excellent agreement of current results with those previously published results encourage us to use the present code.

Pr	A	Ibrahim[51]	Ibrahim[55]	Mahapatra[53]	Hayat[56]	Present	
						Shooting	bvp4c
1	0.1	0.6028	0.6022	0.603	0.602156	0.6036	0.6506
	0.2	0.6246	0.6245	0.625	0.624467	0.6185	0.6552
	0.5	0.6924	0.6924	0.692	0.692460	0.6696	0.6849
1.5	0.1	0.7768	0.7768	0.777	0.776802	0.7774	0.7983
	0.2	0.7971	0.7971	0.797	0.797122	0.7867	0.8030
	0.5	0.8684	0.8648	0.863	0.864771	0.8382	0.8357
2.0	0.1	0.9257	-	-	-	0.9291	0.9291
	0.2	0.9447	-	-	-	0.9333	0.9333
	0.5	1.0116	-	-	-	0.9657	0.9657

TABLE 3.2: Comparison of the local Nusselt number $-\theta'(0)$ when $Nt = 0$, $Nb \to 0$, for different values of Pr with formerly published data.

Furthermore, we reproduce the results of [51] for the local Nusselt number $\theta'(0)$. Table 3.3 presents the local Nusselt number $\theta'(0)$ by taking random values of different physical parameters used such as Brownian motion, thermophoresis parameter, Biot number and the velocity ratio. It is observed in the table that the local Nusselt number $\theta'(0)$ is decreasing function of the thermophoresis parameter Nt and an increasing function of the Biot number Bi.

Nt	-θ'				
	$Bi = 0.1$	$Bi = 2$	$Bi = 5$	$Bi = 10$	$Bi = 100$
0.1	0.0861	0.4747	0.5535	0.5860	0.6186
0.2	0.0860	0.4608	0.5317	0.5602	0.5885
0.5	0.0859	0.4398	0.4998	0.5231	0.5456
1.0	0.0857	0.4050	0.4490	0.4652	0.4804
1.5	0.0854	0.3709	0.4021	0.4130	0.4229
2.0	0.0852	0.3381	0.3596	0.3667	0.3721
5.0	0.0834	0.1929	0.1944	0.1949	0.1952
7.0	0.0817	0.1419	0.1422	0.1422	0.1423
10.0	0.0781	0.1001	0.1001	0.1001	0.1001

TABLE 3.3: Computed values of the local Nusselt number $-\theta'(0)$ for the different values of Nt and Bi if $Nb = 5, A = 0.3, Pr = M = 1, Le = 5$

3.5 Graphical Results

In this Section, we analyze the numerical solution of model displayed in the graphical and tabuler form. The calculations have been done for different estimations of velocity ratio, Lewis number, Biot number, magnetic parameter, thermophoresis, Prandtl number, Brownian motion, and the effects of these parameters on the velocity, temperature and concentration profiles have also been discussed.

3.5.1 Impact of Velocity Ratio Parameter on the Velocity

Figure 3.2 designates that by enlarging A ($A > 1$), the width of the hydrodynamic boundary layer increases, and it declines by decreasing A ($A < 1$). Physically, the ratio between free stream velocity and the stretching velocity is greater than 1 if stretching velocity becomes less than the free stream velocity. Consequently, flow velocity is increased whereas retarding force is declined.

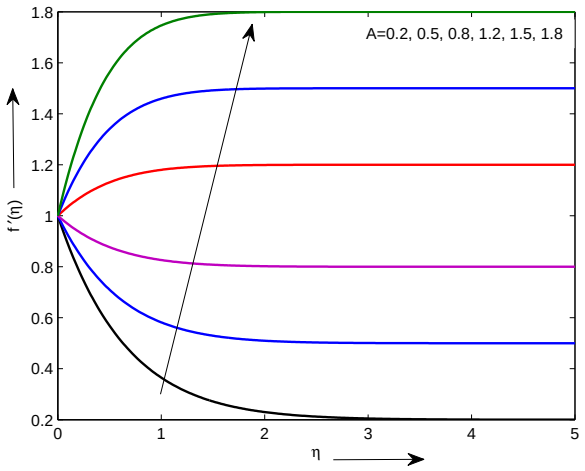

FIGURE 3.2: Velocity profile vs A when $Le = Bi = 5$, $Nb = Nt = 0.5$ and $M = Pr = 1$.

3.5.2 Impact of Magnetic Parameter on the Velocity

Figure 3.3 divulges the impact of magnetic parameter on the velocity f'. Here, due to magnetic field an opposing force which is called Lorentz force, appears which resist the flow of fluid and consequently the flow of velocity declines.

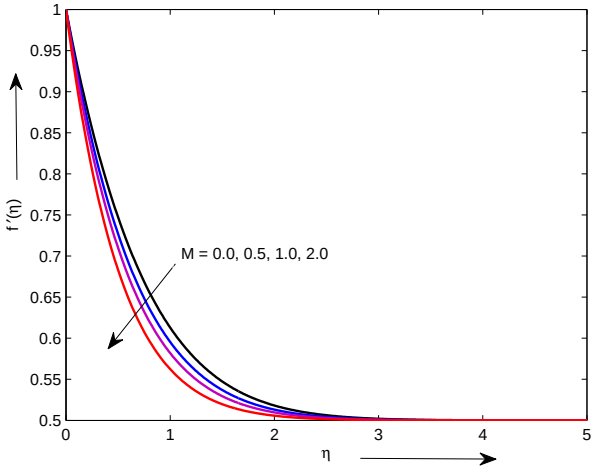

FIGURE 3.3: Velocity profile vs M when $Nt = A = Nb = 0.5$, $Le = Bi = 5$ and $Pr = 1$.

3.5.3 Impact of Prandtl Number on the Temperature

Figure 3.4 designates the impact of Pr on the temperature profile $\theta(\eta)$. It is clear from figure that the temperature of the flow field is the decreasing function of Pr. It is because of the way when Pr of fluid is high then thermal diffusion is low if it is compared with

the viscous diffusion. Consequently, the coefficient of heat transfer declines as well as shrinks the thickness of the boundary layer.

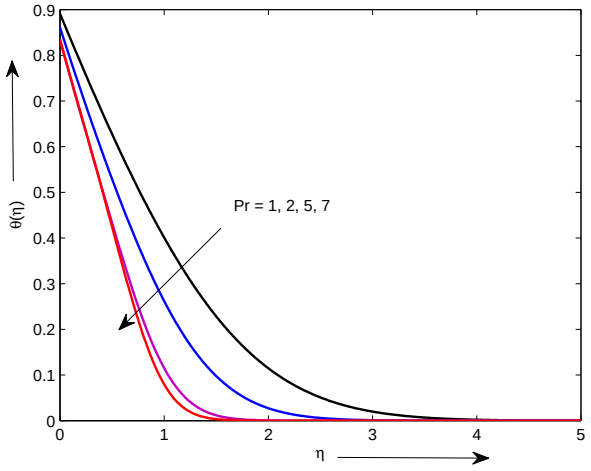

FIGURE 3.4: Temperature profile vs Pr as $Nt = 0.5$, $A = Nb = 0.5$, $Le = Bi = 5$ and $M = 1$.

3.5.4 Impact of Thermophoresis Parameter on the Temperature

Figure 3.5 delineates the influence of Nt on the temperature profile. When the effects of thermophoretic increase, the relocation of the nanoparticles relocate from hot part of the surface to the cold ambient fluid and consequently, at the boundary, temperature is increased. This sequels in the thickening of thermal boundary layer.

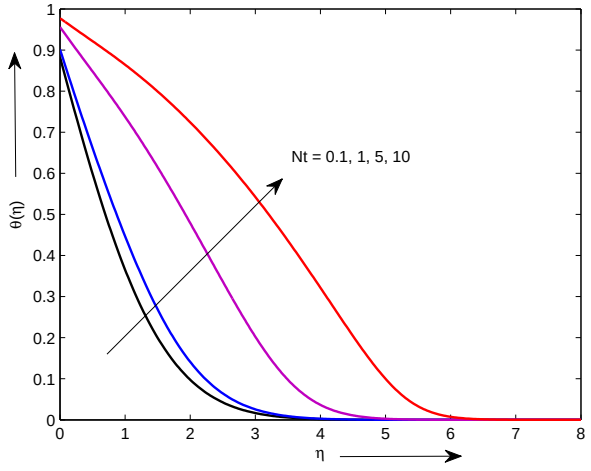

FIGURE 3.5: Temperature profile vs Nt when $Pr = M = 1$, $Nb = A = 0.5$ and $Le = Bi = 5$.

3.5.5 Impact of Convective Heating on the Temperature

Figure 3.6 describes the effect of the convective heating which is also known as the Biot number on the temperature profile $\theta(\eta)$. Numerically, it can be calculated by dividing the convection on the surface to the conduction into the surface of an object. When Bi increases, it causes increase in the temperature on surface which sequels in the thickening of the thermal boundary layer.

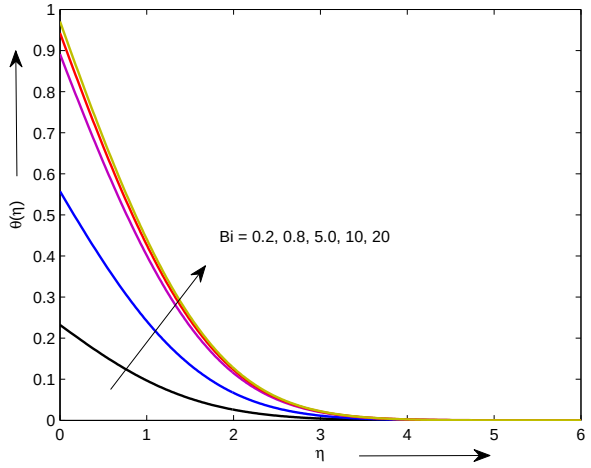

FIGURE 3.6: Temperature profile vs Bi when $Nb = A = Nt = 0.5$, $Pr = M = 1$, $Le = 5$.

3.5.6 Impact of Velocity Ratio Parameter on the Temperature

The effect of velocity ratio parameter A on the temperature profile $\theta(\eta)$ has been highlighted by Figure 3.7. As we increase the value of velocity ratio parameter A, the temperature at the surface declines, and furthermore, it also declines the thickness of the thermal boundary layer.

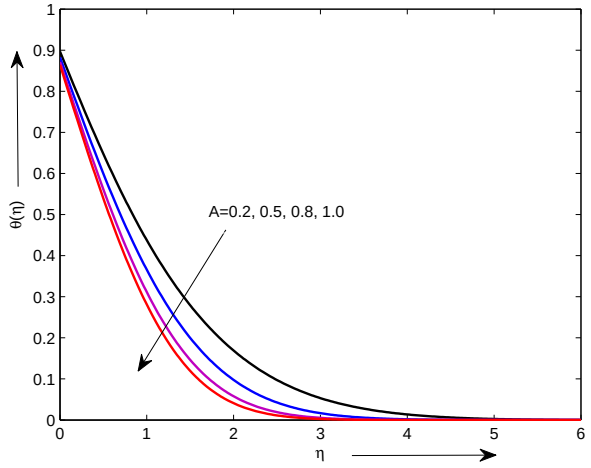

FIGURE 3.7: Temperature profile vs A when $Nb = Nt = 0.5$, $Pr = M = 1$, and $Le = Bi = 5$.

3.5.7 Impact of Brownian Motion Parameter on the Concentration

The impact of the Brownian motion parameter Nb on the concentration $\phi(\eta)$ is illustrated by Figure 3.8. When we increase the effect of Bi, the concentration profile $\phi(\eta)$ also increases initially but it starts decreasing faraway from the wall.

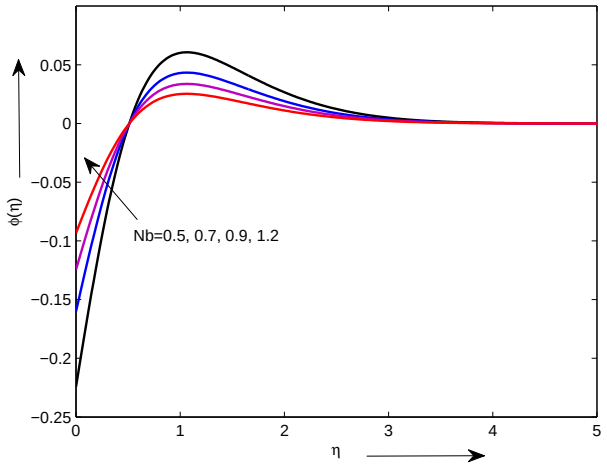

FIGURE 3.8: Concentration profile vs Nb when $Pr = M = 1$, $Nt = A = 0.5$, and $Bi = Le = 5$.

3.5.8 Impact of Thermophoresis Parameter on the Concentration

It seems clearly from the Figure 3.9 that if we increase the thermophoretic force, it cause decline in the concentration profile $\phi(\eta)$ at the surface, which is reverse in nature to the case of the Bi.

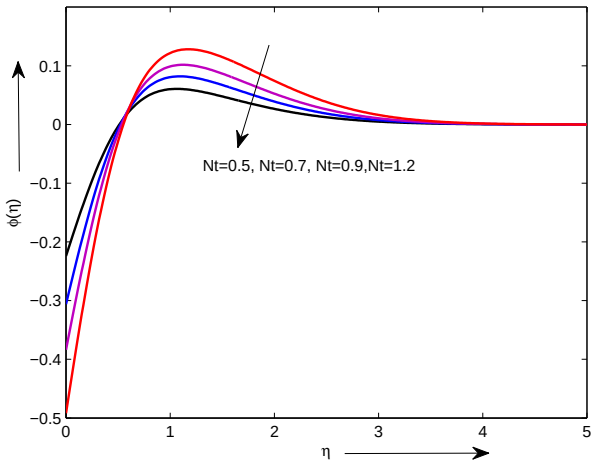

FIGURE 3.9: Concentration profile vs Nt when $Nb = A = 0.5$, $M = Pr = 1$ and $Le = Bi = 5$.

3.5.9 Impact of Lewis Number on the Concentration

The concentration vs Lewis number has been illustrated by Figure 3.10. Increasing Le corresponding to the concentration. As a result, initially the concentration on surface increases but after a while, a bit away from the surface it starts decreasing.

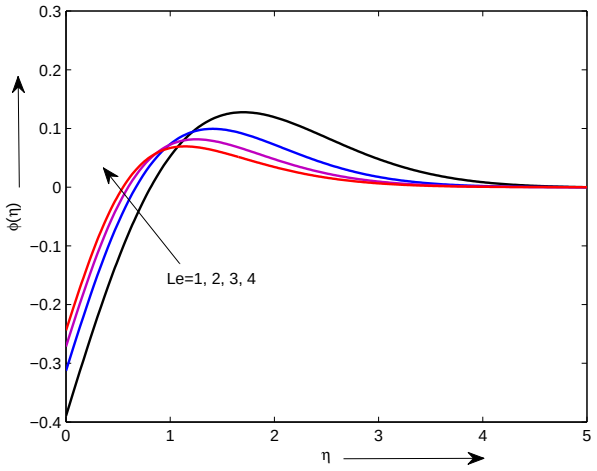

FIGURE 3.10: Concentration profile vs Le when $Nt = A = Nb = 0.5$, $Pr = M = 1$ and $Bi = 5$.

3.5.10 Impact of Velocity Ratio Parameter on the Concentration

Figure 3.11 demonstrates the concentration vs velocity ratio. It has the similar effects on the concentration profile as the effect of Lewis number is noted on concentration. As the concentration distribution decreases by increasing the velocity ratio parameter A .

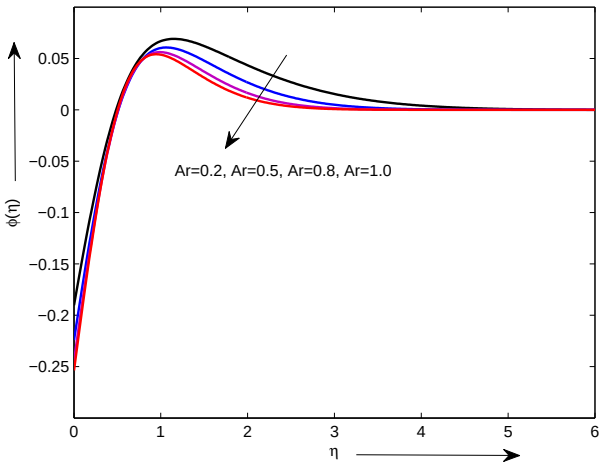

FIGURE 3.11: Concentration profile vs A when $Nt = Nb = 0.5$, $Pr = M = 1$ and $Bi = Le = 5$.

Chapter 4

CHEMICAL REACTION AND INTERNAL HEAT SOURCE EFFECTS ON MHD NANOFLUID OVER A STRETCHING SHEET

4.1 Introduction

In this chapter, we will extend the flow model of Ibrahim and Haq [51], which was presented in the foregoing chapter by considering the "MHD stagnation point flow of steady, two-dimensional viscous flow of the nanofluid over a stretching surface along with the convective boundary condition". Here, we will scrutinize the "Chemical reaction and non-uniform internal heat source effects on the MHD mixed convection stagnation point flow of Maxwell nanofluid over a stretching surface". At the lower surface of the system, the sheet is continuously heated with the temperature T_f and the heat transfer coefficient h_f as discussed in Chapter 3. The system of three coupled, nonlinear PDEs of momentum, energy and concentration is transmuted into system of ODEs by using an appropriate similarity transformation. We use the shooting technique to obtain the numerical solution of this converted BVP. Finally, at the end of this Chapter the results

are tabulated for many physical parameters affecting the MHD mixed convection flow and found to be in very good agreement with those obtained by using the MATLAB software bvp4c. Significance of different parameters which governs the flow on the velocity, temperature and concentration are elaborated at the end of this Chapter through various graphs and tables.

4.2 Problem Formulation

We consider the magnetohydrodynamic boundary layer flow of Maxwell nanofluid near the stagnation point over a stretching surface with mixed convection. The coordinates

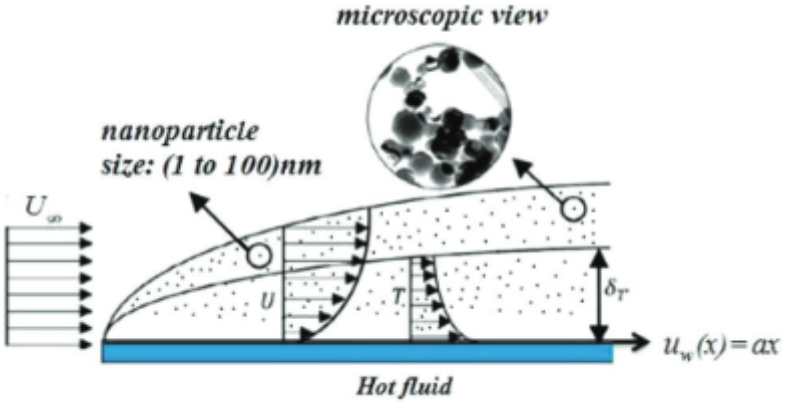

FIGURE 4.1: Geometry for the flow under consideration.

system has been chosen in such a way that $x-$axis is in the direction of the stretching surface and $y-$axis is in the direction normal to the surface. Assume that there isn't any flux of nanoparticles at surface. The impact of the thermophoresis has been considered in the boundary conditions. At the surface, the velocity of stretching surface is $u_w(x) = ax$, where "a" is some constant. The flow is directed to a transverse magnetic field B_0 which is supposed to be applied in the direction of positive $y-$axis, perpendicular to the surface. Extending the idea of Ibrahim and Haq [51], the governing PDEs of the MHD mixed convection stagnation point flow of Maxwell nanofluid along with the chemical reaction

and non-uniform internal heat source effects can be written as

$$\frac{\partial u}{\partial x}+\frac{\partial v}{\partial y}=0, \tag{4.1}$$

$$u\frac{\partial u}{\partial x}+v\frac{\partial u}{\partial y}=\upsilon\left(\frac{\partial^2 u}{\partial y^2}\right)+U_\infty\frac{\partial U_\infty}{\partial x}+\frac{\sigma B_o^2}{\rho_f}(U_\infty-u)+\lambda\Bigg[u^2\frac{\partial^2 u}{\partial x^2}+v^2\frac{\partial^2 u}{\partial y^2}+2uv\frac{\partial^2 u}{\partial x\partial y}\Bigg]+g\beta_T(T-T_\infty)+g\beta_C(C-C_\infty), \tag{4.2}$$

$$u\frac{\partial T}{\partial x}+v\frac{\partial T}{\partial y}=\alpha\frac{\partial^2 T}{\partial y^2}+\Gamma\left[D_B\left(\frac{\partial C}{\partial y}\frac{\partial T}{\partial y}\right)+\frac{D_T}{T_\infty}\left(\frac{\partial T}{\partial y}\right)^2\right]+\frac{q'''}{(\rho c)_p}, \tag{4.3}$$

$$u\frac{\partial C}{\partial x}+v\frac{\partial C}{\partial y}=D_B\frac{\partial^2 C}{\partial y^2}+\frac{D_T}{T_\infty}\left(\frac{\partial^2 T}{\partial y^2}\right)-K_1(C-C_\infty). \tag{4.4}$$

Where, q''' represents the temperature and space dependent heat generation and

$$q'''=\frac{Ku_w(x)}{(\rho c)_p x\upsilon}\{A^*(T_f-T_\infty)f'+B^*(T-T_\infty)\}$$

where A^* is space dependent and B^* is temperature dependent heat generation. It is observed that $A^*<0$ and $B^*<0$ mean heat absorption whereas in opposite case they communicate generation. In Eq. (4.4), $K_1(C-C_\infty)$ denotes the chemical reaction term, where K_1 is the chemical reaction parameter. The corresponding BCs for the proposed model are

$$\left.\begin{aligned}&u=u_w=ax, v=0, -k\frac{\partial T}{\partial y}=h_f(T_f-T), D_B\frac{\partial C}{\partial y}+\frac{D_B}{T_\infty}\left(\frac{\partial T}{\partial y}\right)=0 \text{ at } y=0,\\&u\to U_\infty=bx,\ v=0,\ T\to T_\infty,\ C\to C_\infty \text{ as } y\to\infty.\end{aligned}\right\} \tag{4.5}$$

4.3 Dimensionless Form of the Model

To convert the PDEs (4.1)-(4.4) along with the BCs (4.5) into the dimensionless form, we use the similarity transformation [51]:

$$\eta=\sqrt{\frac{a}{\upsilon}}y,\ \psi=\sqrt{a\upsilon}xf(\eta),\ \theta(\eta)=\frac{T-T_\infty}{T_f-T_\infty},\ \phi(\eta)=\frac{C-C_\infty}{C_\infty}. \tag{4.6}$$

In above, $\psi(x,y)$ denotes stream function obeying

$$u=\frac{\partial\psi}{\partial y},\qquad v=-\frac{\partial\psi}{\partial x}. \tag{4.7}$$

The equation of continuity (4.1) is satisfied identically. The governing Eqs. (4.2)-(4.4) are reduced into the following nonlinear ODEs.

$$f''' + ff'' - f'^2 + A^2 + M(A - f') + \beta(f^2 f''' - 2ff'f'') + Gr\theta + Gc\phi = 0, \tag{4.8}$$

$$\theta'' + Pr(f\theta' + Nb\phi'\theta' + Nt\theta'^2) + A^* f' + B^*\theta = 0, \tag{4.9}$$

$$\phi'' + LePrf\phi' + \frac{Nt}{Nb}\theta'' - \gamma LePr\phi = 0. \tag{4.10}$$

The BCs get the form:

$$f'(0) = 1, f(0) = 0,\ Nt\theta'(0) + Nb\phi'(0) = 0,\ \theta'(0) = Bi(\theta(0) - 1),\ \text{at } \eta = 0, \tag{4.11}$$

$$f'(\eta) \to A,\ \theta(\eta) \to 0,\ \phi(\eta) \to 0,\ \text{as } \eta \to \infty. \tag{4.12}$$

In Eqs. (4.8) - (4.12), the governing parameters are defined as

$$\left.\begin{aligned} &Gr = \frac{g\beta_T}{a^2 x}(T_f - T_\infty),\ Gc = \frac{g\beta_C}{a^2 x}C_\infty,\ LePr = Sc = \frac{\upsilon}{D_B}, \\ &A = \frac{b}{a},\ Pr = \frac{\mu C_p}{K},\ \gamma = \frac{K_1}{a},\ \beta = \lambda a,\ M = \sigma\frac{{B_o}^2}{\rho_f a}, \\ &Nb = \frac{(\rho c)_p D_B C_\infty}{(\rho c)_f \upsilon},\ Nt = \frac{(\rho c)_p D_T (T_f - T_\infty)}{(\rho c)_f \upsilon T_\infty}. \end{aligned}\right\} \tag{4.13}$$

In this problem, the desired physical quantities are the local Nusselt number Nu_x and the skin-friction coefficient C_f. These quantities are defined as

$$C_f = \frac{\tau}{\rho {u_w}^2},\ Nu_x = \frac{xq_w}{k(T_f - T_\infty)}. \tag{4.14}$$

Here, the wall heat flux q_w, and the wall shear stress τ_w, are given as

$$\tau_w = \mu\left(\frac{\partial u}{\partial y}\right)_{y=0},\ q_w = -k\left(\frac{\partial T}{\partial y}\right)_{y=0}. \tag{4.15}$$

With the help of above equations, we get

$$C_f\sqrt{Re_x} = -f''(0),\ \frac{Nu_x}{\sqrt{Re_x}} = -\theta'(0). \tag{4.16}$$

Here $Re_x = \frac{ax^2}{\upsilon}$ represents Reynolds number whereas Nu_x represents the local Nusselt number.

4.4 Numerical Results

In this Section, the scheme for the numerical solution of the system of three coupled ODEs (4.8)-(4.10) with BCs (4.11)-(4.12) will be discussed. Because of its efficiency, the shooting technique has been prefered to apply. First, the system of equations (4.8)-(4.10) will be transmuted into a system of ODEs. We can write

$$f''' = \frac{1}{1+\beta f^2}\big[f'^2 - ff'' - A^2 - M(A-f') + 2\beta f f' f'' - Gr\theta - Gc\phi\big], \tag{4.17}$$

$$\theta'' = -Pr\big[f\theta' + Nb\theta'\phi' + Nt\theta'^2\big] - A^* f' - B^*\theta, \tag{4.18}$$

$$\phi'' = \gamma LePr\phi - LePrf\phi' + \frac{Nt}{Nb}\big[Pr(f\theta' + Nb\theta'\phi' + Nt\theta'^2) + A^* f' + B^*\theta\big]. \tag{4.19}$$

By using the following notations

$$f = y_1,\ f' = y_2,\ f'' = y_3,\ \theta = y_4,\ \theta' = y_5,\ \phi = y_6,\ \phi' = y_7, \tag{4.20}$$

the above system of coupled nonlinear ODEs is converted into the following system of seven first order equations:

$$\begin{aligned}
y_1' &= y_2,\\
y_2' &= y_3,\\
y_3' &= \frac{1}{1+\beta y_1^2}\big[y_2^2 - y_1y_3 - A^2 - M(A-y_2) + 2\beta y_1y_2y_3 - Gry_4 - Gcy_6\big],\\
y_4' &= y_5,\\
y_5' &= -Pr\big[y_1y_5 + Nby_5y_7 + Nty_5^2\big] - A^*y_2 - B^*y_4,\\
y_6' &= y_7,\\
y_7' &= \gamma LePry_6 - LePry_1y_7 + \frac{Nt}{Nb}\big[Pr(y_1y_5 + Nby_5y_7 + Nty_5^2) + A^*y_2 + B^*y_4\big].
\end{aligned}$$

The resulting form of the boundary conditions is

$$\begin{aligned}
&y_1(0) = 0,\ y_2(0) = 1,\ y_5(0) = Bi(y_4(0) - 1),\ y_7(0) = -\frac{Nt}{Nb}y_5(0),\\
&y_2 \to A,\ y_4 \to 0,\ y_6 \to 0 \text{ as } \eta \to \infty.
\end{aligned}$$

To execute the numerical procedure, the unbounded domain $[0,\infty)$ has been replaced by $[0,\eta_{max}]$ for some suitable choice of η_{max}. An asymptotic convergence of the numerical

solution is observed by increasing the value of η_{max}. The shooting method requires some initial guess for $y_3(\eta)$, $y_4(\eta)$ and $y_6(\eta)$ at $\eta = 0$. The initial guess is updated by the Newton's method until a solution of the problem which approximately meets the given boundary conditions at the right end of the domain. To validate the MATLAB code, we set $\beta = 0$, $Gr = 0$, $Gc = 0$, $A^* = 0$, $B^* = 0$ and $\gamma = 0$, and obtain exactly the same results and graphs as discussed in Chapter 3. The physical parameters, the local skin-friction coefficient C_f and the local Nusselt number Nu_x, are of great interest for engineers and mathematicians. The skin-friction coefficient examines the viscous stress acting on the surface of the body whereas the local Nusselt number Nu_x is the ratio between the convective heat transfer and the conductive heat transfer at the surface of the body.

						$-f''(0)$		$-\theta'(0)$	
A	M	β	γ	Le	Bi	Shooting	bvp4c	Shooting	bvp4c
0.1	1.0	0.6	0.6	0.2	0.2	1.243941	1.243942	0.325186	0.325186
0.2						1.189946	1.189946	0.591051	0.591051
0.3						1.242064	1.242064	1.484108	1.484108
	0.5					1.084907	1.084908	0.395633	0.395631
	1.0					1.243941	1.243942	0.325186	0.325186
	1.5					1.390760	1.390760	0.288612	0.288611
		0.4				1.277225	1.277225	0.304179	0.304180
		0.6				1.243941	1.243942	0.325186	0.325186
		0.8				1.211603	1.211603	0.351818	0.351817
			0.0			1.227885	1.227886	0.331895	0.331895
			0.6			1.243941	1.243942	0.325186	0.325186
			0.9			1.247504	1.247504	0.323943	0.323943
				0.2		1.243941	1.243942	0.325186	0.325186
				0.6		1.254848	1.254849	0.321263	0.321263
				1.0		1.258224	1.258224	0.321617	0.321617
					0.1	1.240617	1.240617	0.165669	0.165670
					0.2	1.243941	1.243942	0.325186	0.325186
					0.3	1.247096	1.247096	0.478489	0.478489

TABLE 4.1: Numerical results of -$f''(0)$ and -$\theta'(0)$ for different values of A, M, β, γ, Le and Bi with $Gr = Gc$=0.1, Pr=1.0, $Bn = Nt$=0.3, A^*=0.4, B^*=0.7

							$-f''(0)$		$-\theta'(0)$	
Gr	Gc	Pr	Nb	Nt	$A*$	$B*$	Shooting	bvp4c	Shooting	bvp4c
0.1	0.1	1.0	0.3	0.3	0.4	0.7	1.243941	1.243942	0.325186	0.325186
0.0							1.179313	1.179314	0.405135	0.405135
0.1							1.243941	1.243942	0.325186	0.325186
0.2							1.278005	1.278006	0.284902	0.284902
	0.1						1.243941	1.243942	0.325186	0.325186
	0.2						1.224684	1.224684	0.342247	0.342247
	0.3						1.201199	1.201200	0.361681	0.361682
		1.0					1.243941	1.243942	0.325186	0.325186
		3.0					1.185067	1.185066	0.075197	0.075197
		5.0					1.197508	1.197508	0.131813	0.131813
			0.3				1.243941	1.243942	0.325186	0.325186
			0.5				1.250604	1.250604	0.318870	0.318870
			0.7				1.253289	1.253290	0.316238	0.316238
				0.0			1.255546	1.255546	0.297469	0.297469
				0.1			1.252189	1.252189	0.305726	0.305719
				0.3			1.243941	1.243942	0.325186	0.325186
					0.1		1.222541	1.222541	0.232237	0.232239
					0.2		1.230012	1.230013	0.264929	0.264932
					0.4		1.243941	1.243942	0.325186	0.325186
						0.7	1.243941	1.243942	0.325186	0.325186
						0.8	1.232713	1.232713	0.271875	0.271875
						0.9	1.225808	1.225809	0.237573	0.237573

TABLE 4.2: Numerical results of -$f''(0)$ and -$\theta'(0)$ for different values of Gr, Gc, Pr, Nb, Nt, A^* and B^* with A=0.1, M=1.0, $\beta = \gamma$=0.6, $Le = Bi$=0.2

Table 4.1 and 4.2 include the numerical values of C_f and Nu_x denoted by $-f''(0)$ and $-\theta'(0)$ respectively, for different physical parameters. The results obtained by the shooting method and the MATLAB in-built solver bvp4c can be found in a very good agrement with each other. It is observed that increasing the values of the magnetic parameter, thermal Grashof number, Brownian motion parameter, space dependent heat generation/absorption coefficient, chemical reaction parameter, Lewis number, Biot number,

enhances the local skin-friction coefficient. Furthermore, the skin friction coefficient decreases by enlarging the values of visco-elastic parameter, solutal Grashof number, thermophoresis parameter, time dependent heat generation/absorption coefficient, whereas it shows a mixed behaviour by increasing the velocity ratio parameter and Prandtl number. The Nusselt number shows an increasing behavior for the velocity ratio parameter, the visco-elastic parameter, the solutal Grashof number, the thermophoresis parameter, the space dependent heat generation/absorption coefficient and the Biot number. It shows a decreasing behaviour for the magnetic parameter, the thermal Grashof number, the Brownian motion parameter, the time dependent heat generation/absorption coefficient and the chemical reaction parameter. It is also noticed that the Nusselt number shows a mixed behaviour for Prandtl number and Lewis number.

4.5 Graphical Results

The objective is to inspect governing parameters on the velocity, temperature and concentration distribution in this Section.

4.5.1 Velocity ratio parameter

Figure 4.2 designates that by increasing the value of A ($A > 1$), the thickness of hydrodynamic boundary layer increases, and it decreases by decreasing the value of A ($A < 1$). Physically, when the free stream velocity is more than the stretching velocity, the ratio between the free stream velocity and the stretching velocity is greater than 1, consequently, it decline the retarding force and increase the flow velocity. The impact of velocity ratio on the temperature $\theta(\eta)$ has been highlighted by Figure 4.3. As the value of the velocity ratio is increased, the temperature of the surface decreases at the surface and furthermore, the thickness of thermal boundary layer declines. Figure 4.4 demonstrates the concentration profile $\phi(\eta)$ under the influence of the velocity ratio parameter. It has the decreasing effects on the concentration profile near the wall. It increases a little bit away from the wall and a little further away from the wall it starts decreasing again.

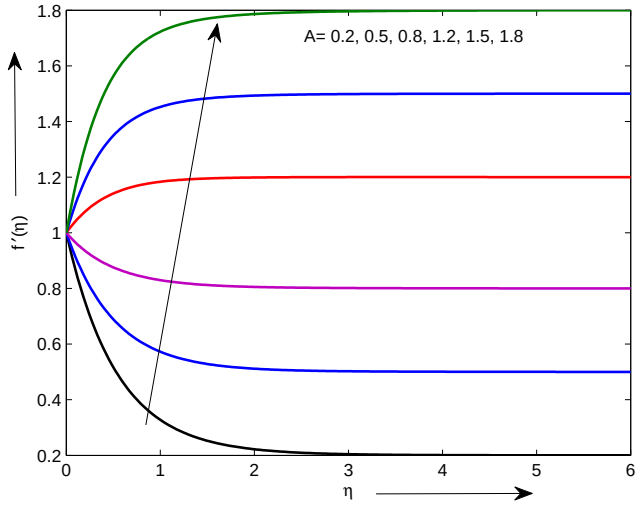

FIGURE 4.2: Dimensionless Velocity vs A when $M = 2.5$, $Pr = 2$, $Nb = Nt = 0.5$, $Le = 5$, $Bi = 5$, $\beta = 0.2$, $A^* = 0.1$,$B^* = 0.2$, $\gamma = 0.5$, $Gr = 0.1$ and $Gc = 0.1$.

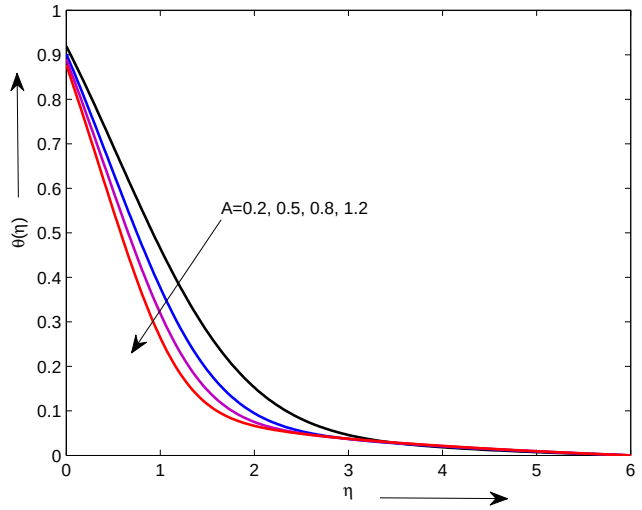

FIGURE 4.3: Dimensionless temperature vs A when $M = 2.5$, $Pr = 2$, $Nb = Nt = 0.5$, $Le = 5$, $Bi = 5$, $\beta = 0.2$, $A^* = 0.1$, $B^* = 0.2$, $\gamma = 0.5$, $Gr = 0.1$ and $Gc = 0.1$.

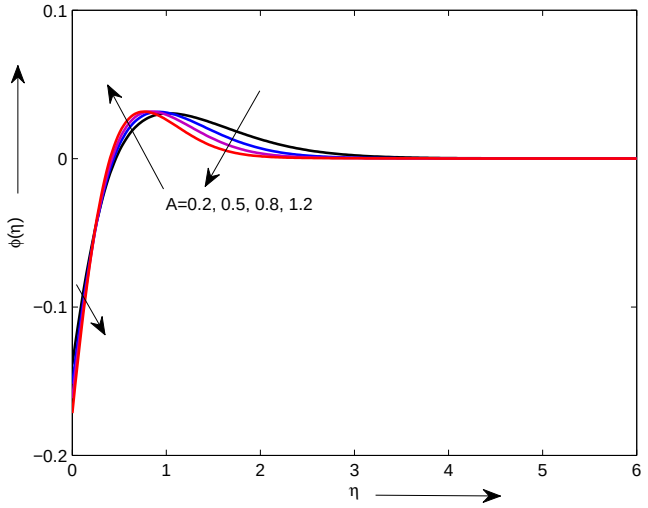

FIGURE 4.4: Dimensionless concentration vs A when $M = 2.5$, $Pr = 2$, $Nb = Nt = 0.5$, $Le = 5$, $Bi = 5$, $\beta = 0.2$, $A^* = 0.1$, $B^* = 0.2$, $\gamma = 0.5$, $Gr = 0.1$ and $Gc = 0.1$.

4.5.2 Magnetic Parameter

Figure 4.5 depicts the impact of M on the dimensionless velocity f'. Here, by increasing the value of M, velocity profile gets declines. Figure 4.6 describes the impact of M on the temperature profile. It is shown in Figure 4.6 that by increasing the value of the magnetic parameter, temperature profile $\theta(\eta)$ gets increase. The impact of the magnetic parameter on the dimensionless concentration, is presented in Figure 4.7. The concentration profile is found to increase when the magnetic parameter increases near the surface. It decreases a bit away from the surface and interestingly, it again starts increasing a bit further away from the surface.

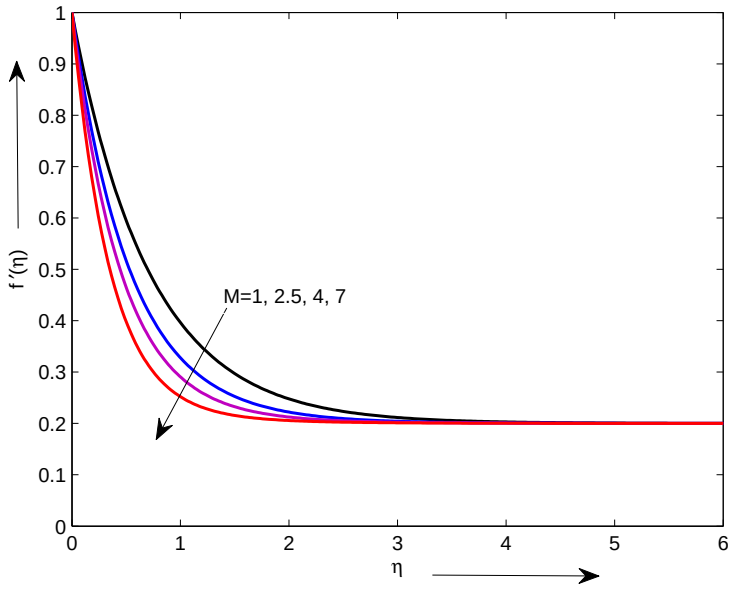

FIGURE 4.5: Dimensionless velocity vs M when $A = 0.2$, $Nb = Nt = 0.5$, $\gamma = 0.5$, $M = 2.5$, $Pr = 2$, $Le = 5$, $Bi = 5$, $\beta = 0.2$, $A^* = 0.1$, $B^* = 0.2$, $Gr = 0.1$ and $Gc = 0.1$.

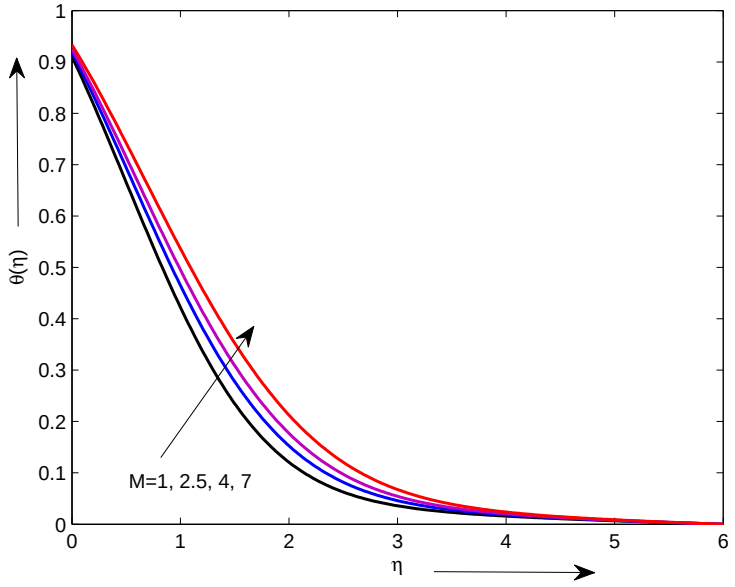

FIGURE 4.6: Dimensionless temperature vs M when $A = 0.2$, $Nb = Nt = 0.5$, $\gamma = 0.5$, $M = 2.5$, $Pr = 2$, $Le = 5$, $Bi = 5$, $\beta = 0.2$, $A^* = 0.1$, $B^* = 0.2$, $Gr = 0.1$ and $Gc = 0.1$.

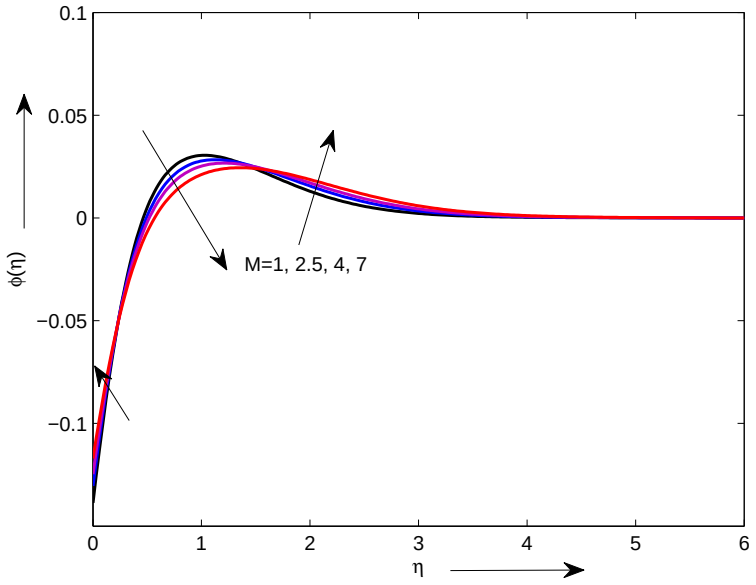

FIGURE 4.7: Dimensionless concentration vs M when $A = 0.2$, $Nb = Nt = 0.5$, $\gamma = 0.5$,$M = 2.5$, $Pr = 2$, $Le = 5$, $Bi = 5$, $\beta = 0.2$, $A^* = 0.1$, $B^* = 0.2$, and $Gr = Gc = 0.1$.

4.5.3 Prandtl Number

Figure It is noticed in the Figure 4.8 the velocity declines by enlarging the Prandtl number. The temperature profile decreases with increasing Prandtl number as depicted in Figure 4.9. The effect of the variation in the Pr on the concentration profile, is observed in Figure 4.10. It is notified from the figure, as the value of Prandtl number rises, the nanoparticles scattered out toward the outward, consequently, the nanoparticles concentration at the surface decreases.

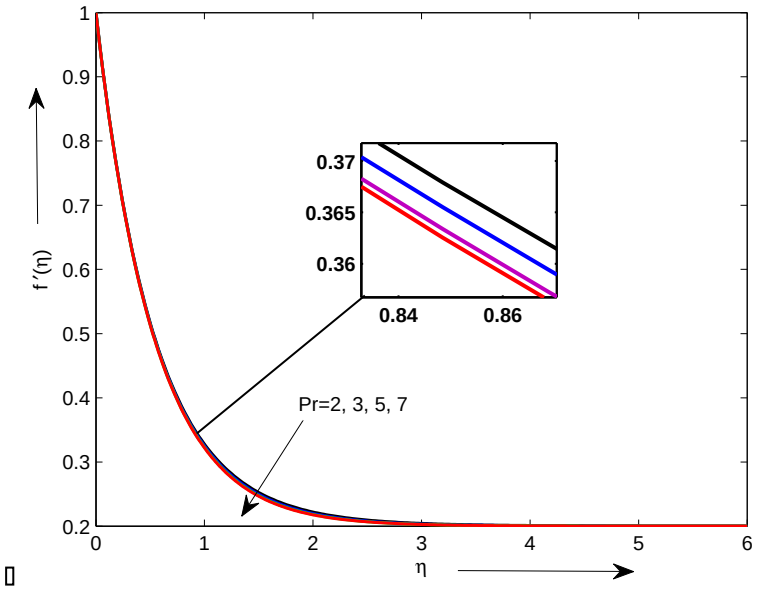

FIGURE 4.8: Dimensionless velocity vs Pr when $A = 0.2$, $Nb = Nt = 0.5$, $\gamma = 0.5$, $M = 2.5$, $Pr = 2$, $Le = 5$, $Bi = 5$, $\beta = 0.2$, $A^* = Gr = 0.1$, $B^* = 0.2$ and $Gc = 0.1$.

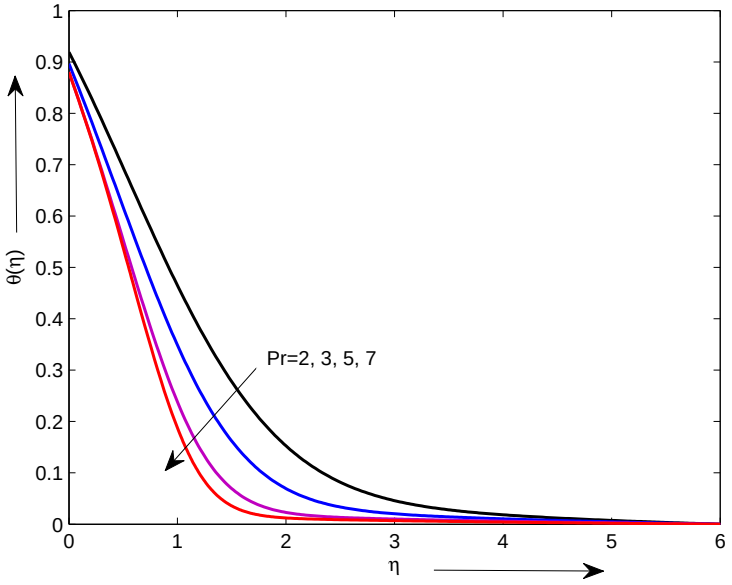

FIGURE 4.9: Dimenssionless temperature vs Pr when $A = 0.2$, $Nb = Nt = 0.5$, $\gamma = 0.5$, $M = 2.5$, $Pr = 2$, $Le = 5$, $Bi = 5$, $\beta = 0.2$, $A^* = Gr = 0.1$, $B^* = 0.2$ and $Gc = 0.1$.

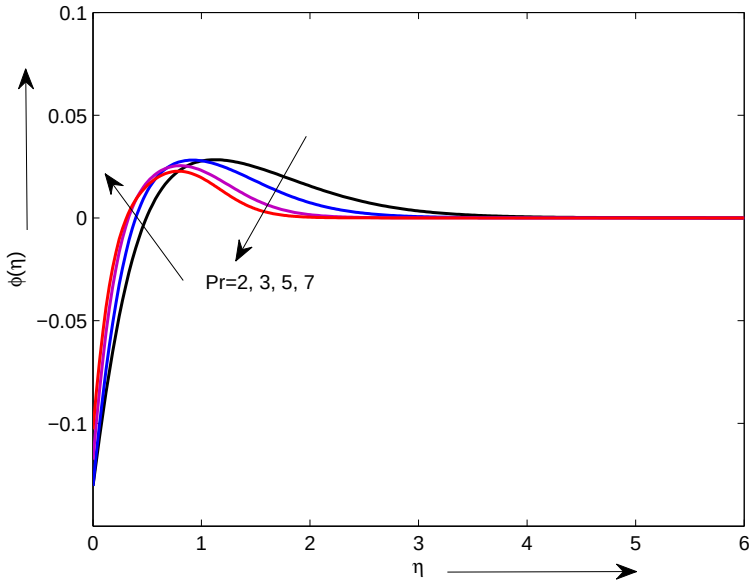

FIGURE 4.10: Dimensionless concentration vs Pr when $A = 0.2$, $Nb = Nt = 0.5$, $\gamma = 0.5$,$M = 2.5$, $Pr = 2$, $Le = 5$, $Bi = 5$, $\beta = 0.2$, $A^* = Gr = 0.1$, $B^* = 0.2$ and $Gc = 0.1$.

4.5.4 Brownian Motion Parameter

Figure 4.11 describes the impact of Brownian motion on the velocity profile. It is noticed in figure that by rising the Brownian motion parameter, a decrease in the dimensionless velocity is resulted. It is noticed from Figure 4.12 that as the value of Nb increases, thickening the thermal boundary layer. The impact of Brownian motion parameter is witness in Figure 4.13 that concentration profile increases by increasing the Nb. Consequently, the Brownian force increases the nanoparticle concentration at the surface. Thus, the concentration profile increases on the surface but it is found to decrease a bit away from the surface.

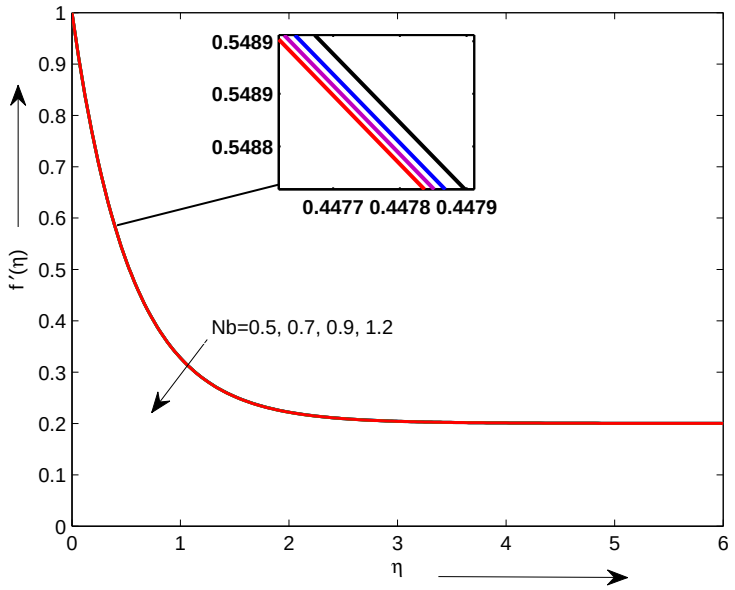

FIGURE 4.11: Dimensionless velocity vs Nb when $A = 0.2$, $Nb = Nt = 0.5$, $\gamma = 0.5$, $M = 2.5$, $Pr = 2$, $Le = 5$, $Bi = 5$, $\beta = 0.2$, $A^* = Gr = 0.1$, $B^* = 0.2$ and $Gc = 0.1$.

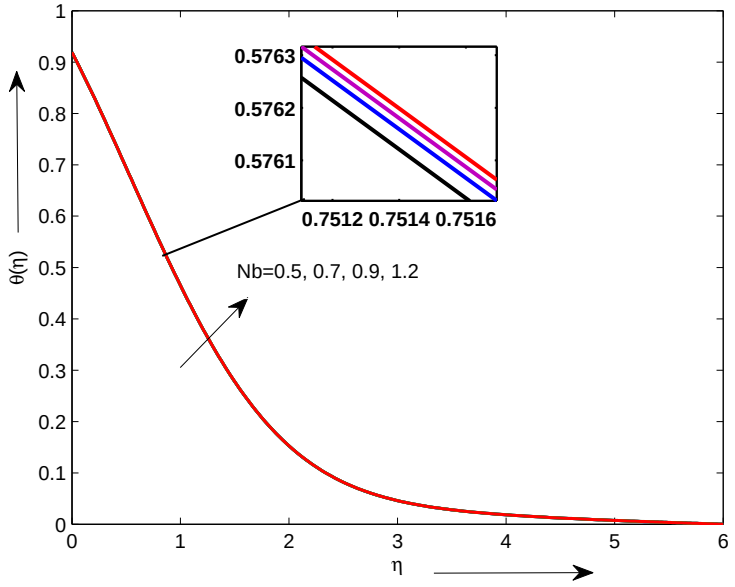

FIGURE 4.12: Dimensionless temperature vs Nb when $A = 0.2$, $Nb = Nt = 0.5$, $\gamma = 0.5$, $M = 2.5$, $Pr = 2$, $Le = 5$, $Bi = 5$, $\beta = 0.2$, $A^* = Gr = 0.1$, $B^* = 0.2$ and $Gc = 0.1$.

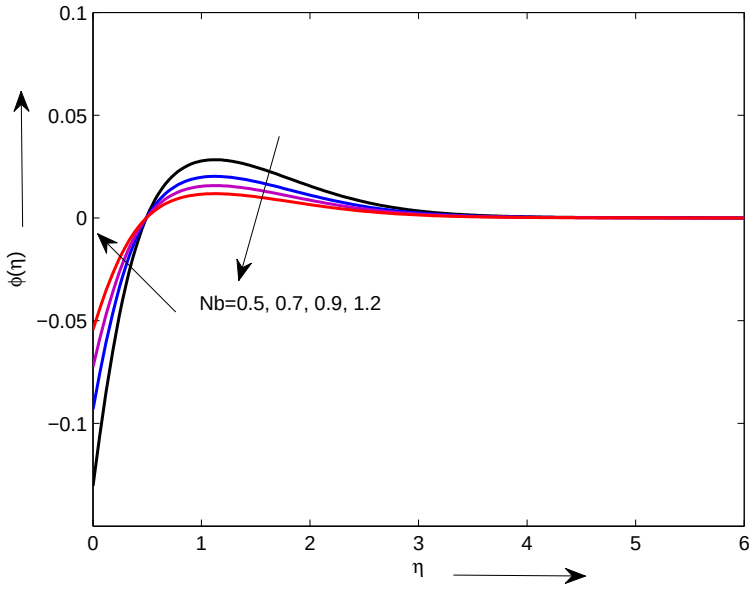

FIGURE 4.13: Dimensionless concentration vs Nb when $A = 0.2$, $Nb = Nt = 0.5$, $\gamma = 0.5$, $M = 2.5$, $Pr = 2$, $Le = 5$, $Bi = 5$, $\beta = 0.2$, $A^* = Gr = 0.1$, $B^* = 0.2$ and $Gc = 0.1$.

4.5.5 Thermophoresis Parameter

Through Figure 4.14, it can be noticed that by enlarging the thermophoresis parameter, thickness of boundary layer also increases, which causes an increase in the velocity profile f'. Figure 4.15 includes the graphs of the temperature distribution in thermal boundary layer for various value of the Nt. It is noticed that if the thermophoesis increases, causing an increase in Nt. Figure 4.16 describes the influence of the Nt on the concentration profile. Therefore, when the influence of the thermophoretic force is enlarged, the concentration profile on the surface declines, which is the opposite in nature to that of the case of the Brownian motion but a bit away from the wall it starts increasing.

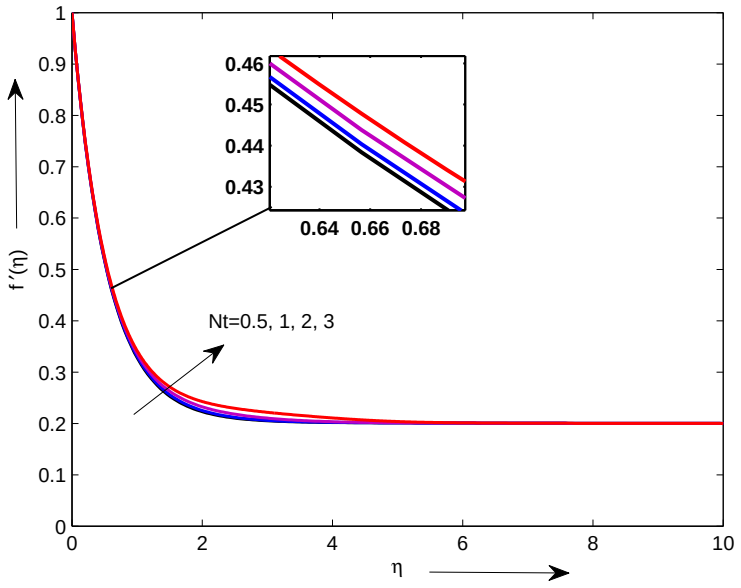

FIGURE 4.14: Dimensionless velocity vs Nt, when $A = B^* = 0.2$, $Nb = 0.5, Nt = 0.5$, $M = 2.5$, $Pr = 2$, $Le = 5$, $Bi = 5$, $\beta = 0.2$, $A^* = Gr = 0.1$, $\gamma = 0.5$, and $Gc = 0.1$.

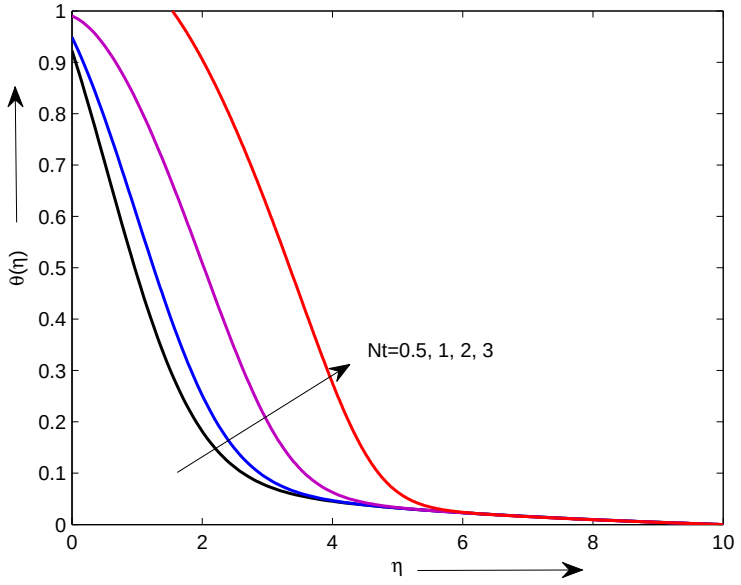

FIGURE 4.15: Dimensionless temperature vs Nt, when $A = 0.2$, $Nb = Nt = 0.5$, $\gamma = 0.5$, $M = 2.5$, $Pr = 2$, $Le = 5$, $Bi = 5$, $\beta = 0.2$, $A^* = Gr = 0.1$, $B^* = 0.2$ and $Gc = 0.1$.

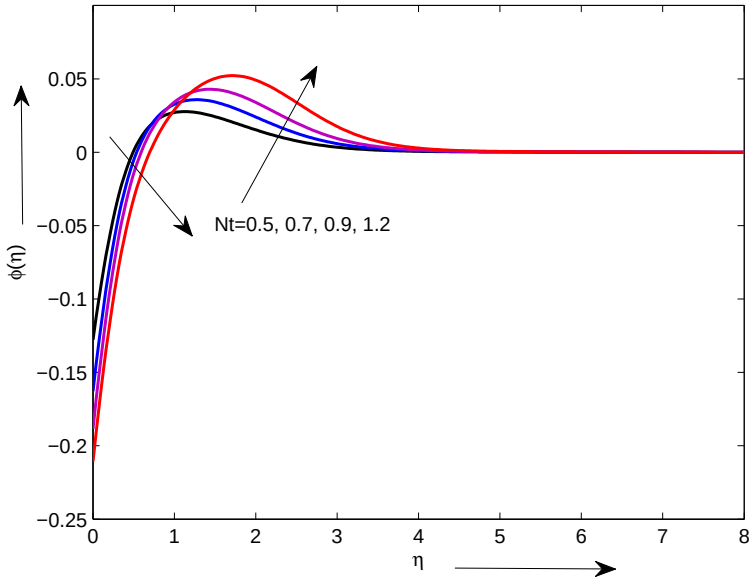

FIGURE 4.16: Dimensionless concentration vs Nt, when $A = B^* = 0.2$, $Nb = Nt = 0.5$, $M = 2.5$, $Pr = 2$, $Le = 5$, $Bi = 5$, $\beta = 0.2$, $A^* = Gr = 0.1$, $\gamma = 0.5$ and $Gc = 0.1$.

4.5.6 Lewis Number

Figure 4.17 illustrates that by increasing the Lewis number, the velocity profile increases. Similar effects are shown for the temperature profile in Figure4.18. The impact of Le on the concentration profile is seen in Figure 4.19. Increasing the Lewis number, the concentration profile near the surface increases but a bit away from the surface it starts decreasing by enhancing the influence of the Lewis number Le.

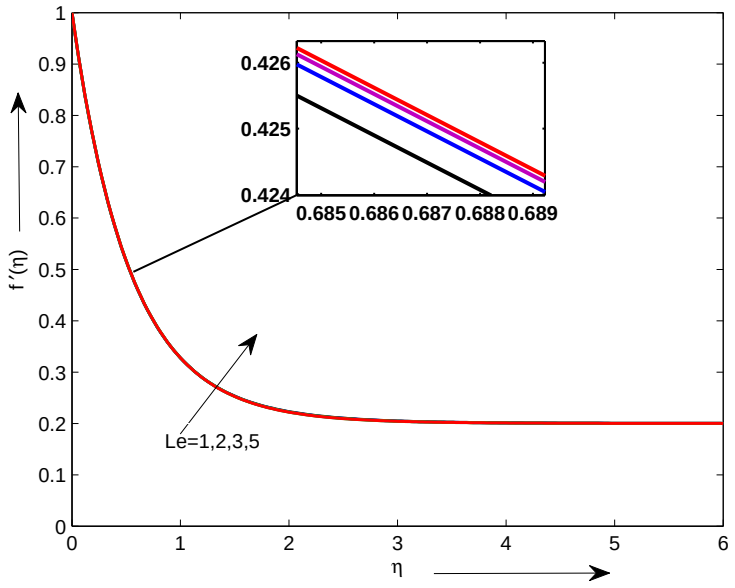

FIGURE 4.17: Dimensionless velocity vs Le when $A = 0.2$, $Nb = Nt = 0.5$, $\beta = 0.2$, $M = 2.5$, $Pr = 2$, $Le = 5$, $Bi = 5$, $A^* = Gr = 0.1$, $B^* = 0.2$, $\gamma = 0.5$ and $Gc = 0.1$.

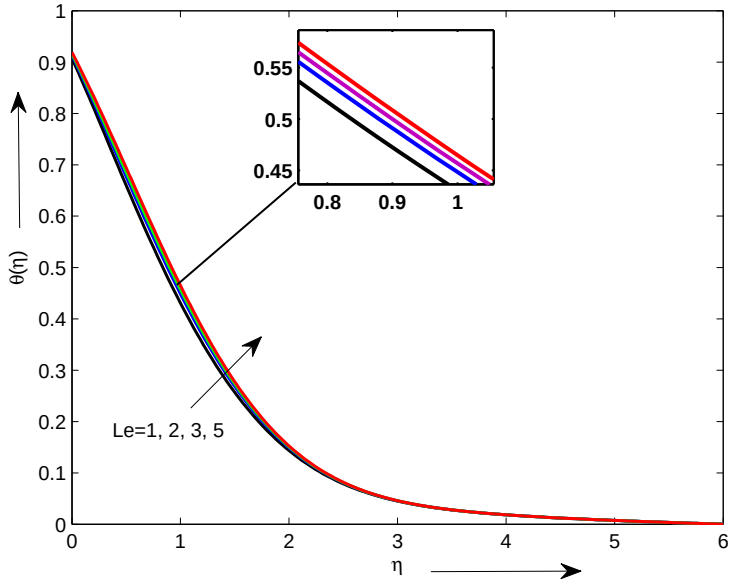

FIGURE 4.18: Dimensionless temperature vs Le when $A = 0.2$, $Nb = Nt = 0.5$, $\beta = 0.2$, $M = 2.5$, $Pr = 2$, $Le = 5$, $Bi = 5$, $A^* = Gr = 0.1$, $B^* = 0.2$, $\gamma = 0.5$ and $Gc = 0.1$.

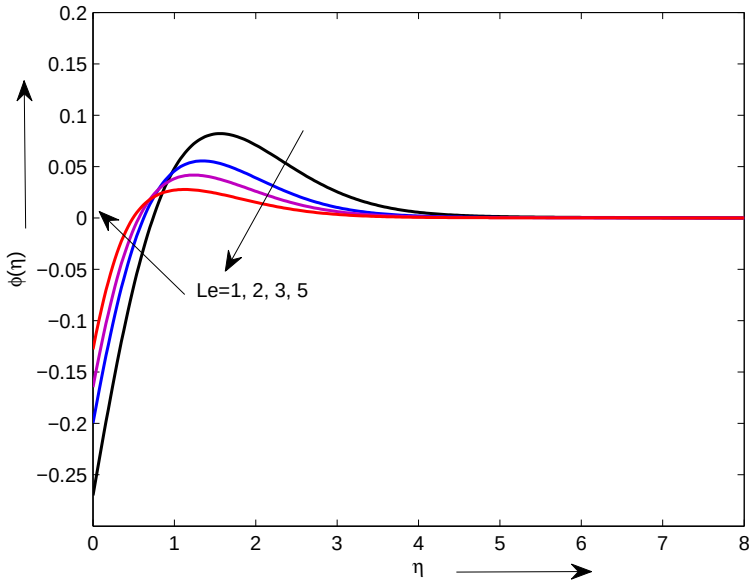

FIGURE 4.19: Dimensionless concentration vs Le when $A = 0.2$, $Nb = Nt = 0.5$, $\beta = 0.2$, $M = 2.5$, $Pr = 2$, $Le = 5$, $Bi = 5$, $A^* = Gr = 0.1$, $B^* = 0.2$, $\gamma = 0.5$ and $Gc = 0.1$.

4.5.7 Biot Number

Figure 4.20 and 4.21 show the influence of convective heating, also known as the Biot number Bi, on the velocity and temperature distribution respectively. Physically, convective heating Bi can be calculated by dividing the convaction at the surface to the conduction on the surface of a body. As an impact of the increasing the Bi, the velocity and temperature on the surface increase, which results thickening of the thermal boundary layer, whereas the Biot number causes a decrease in the concentration profile ϕ, which is indeed reflected in Figure 4.22.

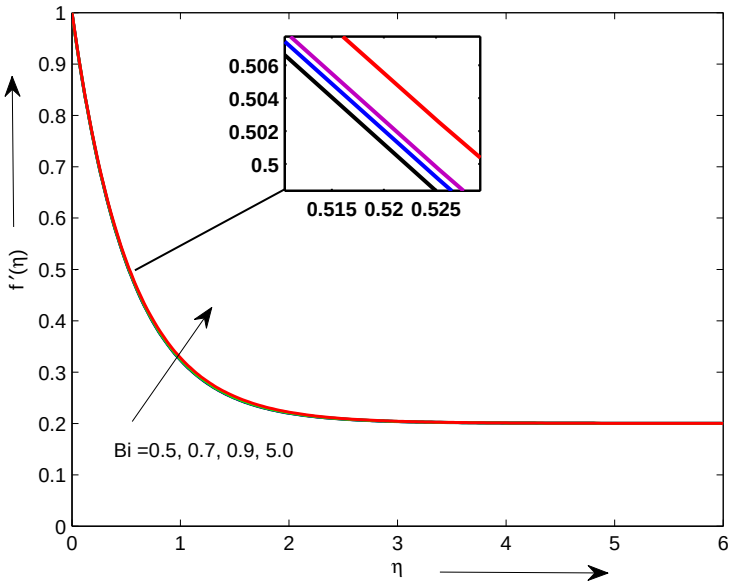

FIGURE 4.20: Dimensionless velocity vs Bi when $A = 0.2$, $Nb = Nt = 0.5$, $\gamma = 0.5$, $M = 2.5$, $Pr = 2$, $Le = 5$, $Bi = 5$, $\beta = 0.2$, $A^* = Gr = 0.1$, $B^* = 0.2$ and $Gc = 0.1$.

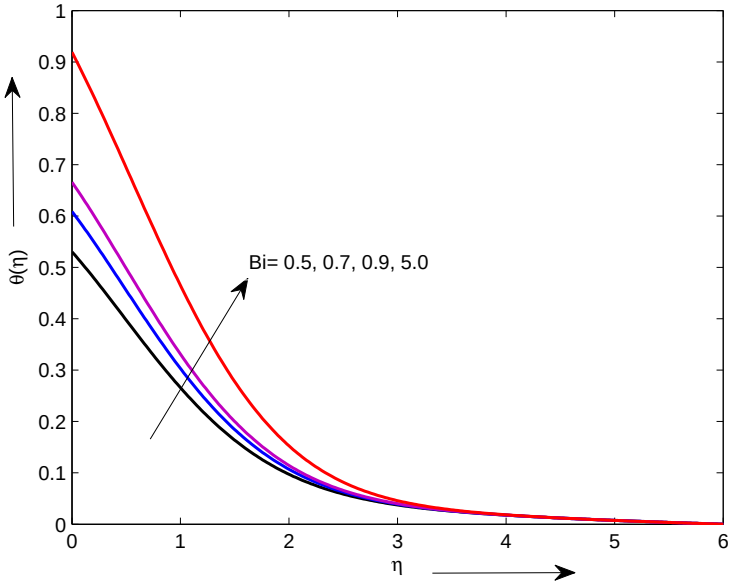

FIGURE 4.21: Dimensionless temperature vs Bi when $A = 0.2$, $Nb = Nt = 0.5$, $\gamma = 0.5$, $M = 2.5$, $Pr = 2$, $Le = 5$, $Bi = 5$, $\beta = 0.2$, $A^* = Gr = 0.1$, $B^* = 0.2$ and $Gc = 0.1$.

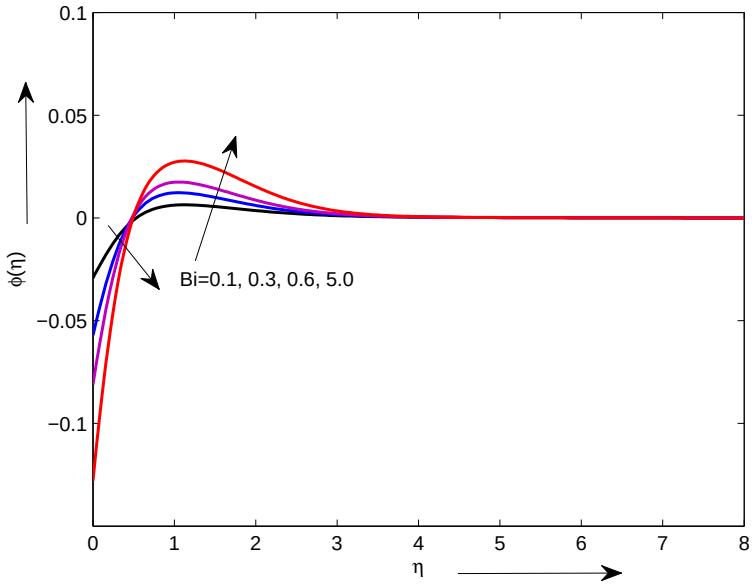

FIGURE 4.22: Dimensionless concentration vs Bi when $A = 0.2$, $Nb = Nt = 0.5$, $\gamma = 0.5$, $M = 2.5$, $Pr = 2$, $Le = 5$, $Bi = 5$, $\beta = 0.2$, $A^* = Gr = 0.1$, $B^* = 0.2$ and $Gc = 0.1$.

4.5.8 Visco-elastic Parameter

It is noticed in Figure 4.23 that as the visco-elastic parameter increases, which causes an increase in the velocity profile. Figure 4.24 depicts exactly the opposite effect of visco-elastic parameter on the temperature profile. The impact of the visco-elastic parameter β on the dimensionless concentration is presented in Figure 4.25. The concentration profile is found to decrease when the visco-elastic parameter increases near the surface. It increases a bit away from the wall and interestingly, it again starts decreasing a bit further away from the surface.

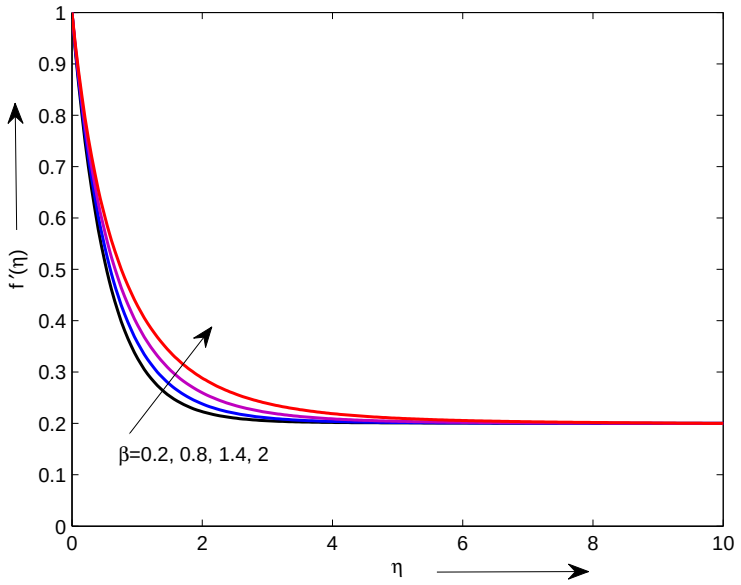

FIGURE 4.23: Dimensionless velocity vs β when $A = 0.2$, $Nb = Nt = 0.5$, $\gamma = 0.5$, $M = 2.5$, $Pr = 2$, $Le = 5$, $Bi = 5$, $\beta = 0.2$, $A^* = Gr = 0.1$, $B^* = 0.2$ and $Gc = 0.1$.

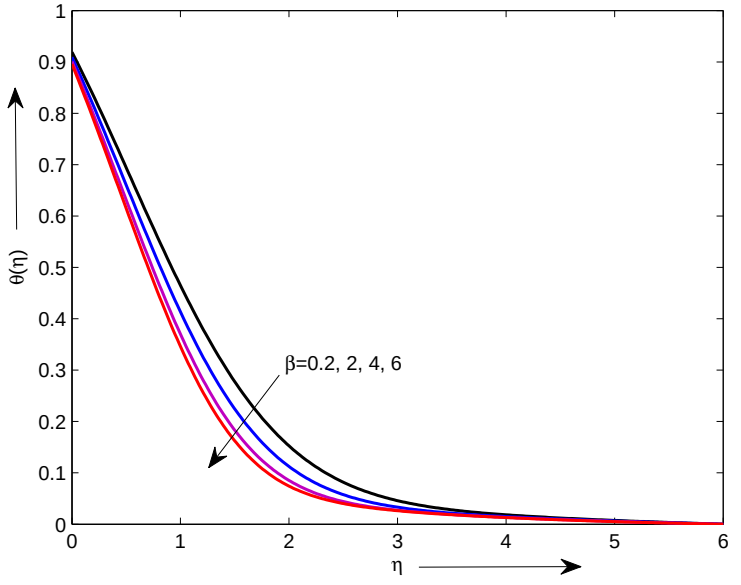

FIGURE 4.24: Dimensionless temperature vs β when $A = 0.2$, $Nb = Nt = 0.5$, $\gamma = 0.5$, $M = 2.5$, $Pr = 2$, $Le = 5$, $Bi = 5$, $\beta = 0.2$, $A^* = Gr = 0.1$, $B^* = 0.2$ and $Gc = 0.1$.

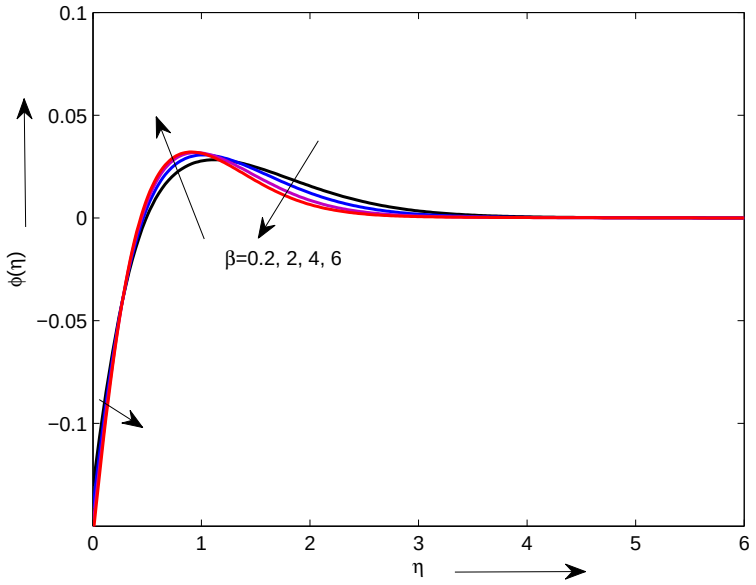

FIGURE 4.25: Dimensionless concentration vs β when $A = 0.2$, $Nb = Nt = 0.5$, $\gamma = 0.5$, $M = 2.5$, $Pr = 2$, $Le = 5$, $Bi = 5$, $\beta = 0.2$, $A^* = Gr = 0.1$, $B^* = 0.2$ and $Gc = 0.1$.

4.5.9 Space Dependent Heat Generation/Absorption Coefficient

It is clear from Figure 4.26 that by enlarging A^*, velocity profile is increased. Figure 4.27 delineates the effect of the A^* on the temperature. The temperature profile is increased by increasing the value of the space dependent heat generation/absorption coefficient A^*. Effect of the space dependent heat generation/absorption coefficient on the concentration is shown in Figure 4.28. Initially, concentration profile increases by increasing the space dependent heat generation/absorption coefficient, it starts decreasing a bit away from the surface. Finally, it again increases a bit further away from the surface.

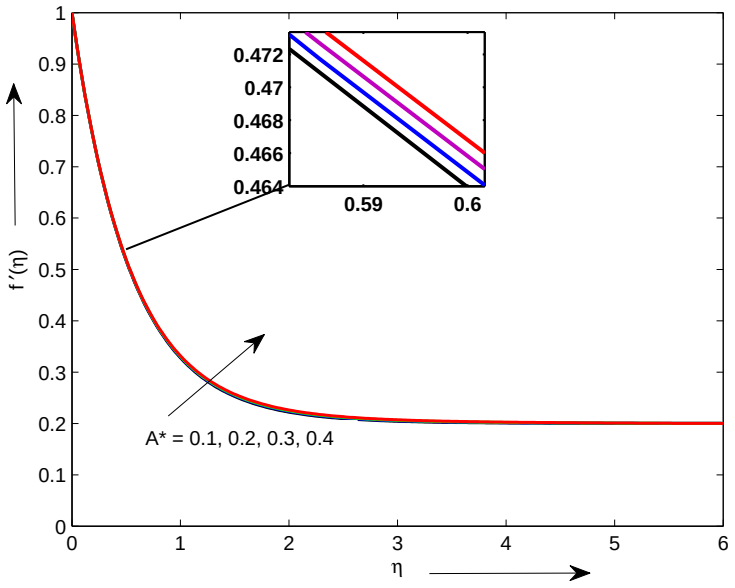

FIGURE 4.26: Dimensionless velocity vs A^* when $A = 0.2$, $Nb = Nt = 0.5$, $\gamma = 0.5$, $M = 2.5$, $Pr = 2$, $Le = 5$, $Bi = 5$, $\beta = 0.2$, $A^* = Gr = 0.1$, $B^* = 0.2$ and $Gc = 0.1$.

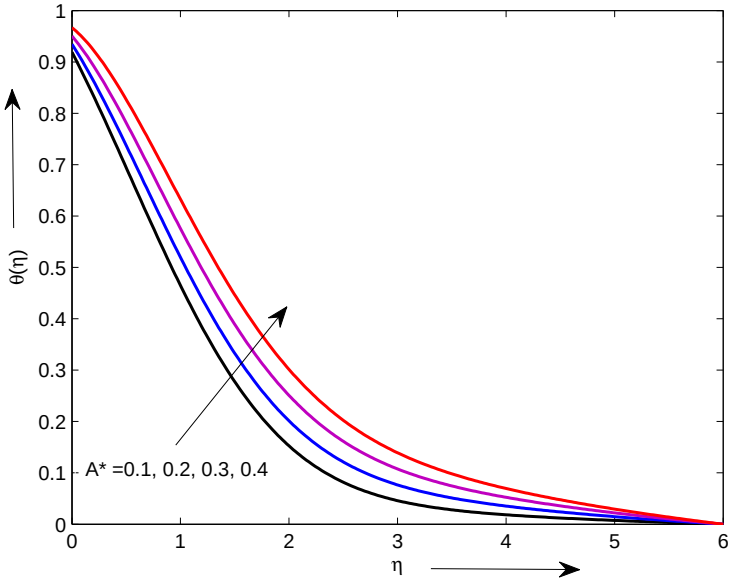

FIGURE 4.27: Dimensionless temperature vs A^* when $A = 0.2$, $Nb = Nt = 0.5$, $\gamma = 0.5$, $M = 2.5$, $Pr = 2$, $Le = 5$, $Bi = 5$, $\beta = 0.2$, $A^* = Gr = 0.1$, $B^* = 0.2$ and $Gc = 0.1$.

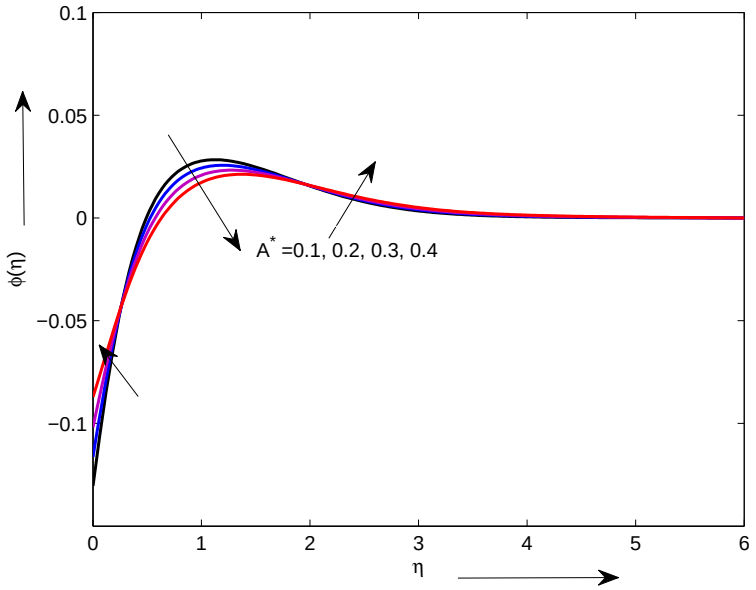

FIGURE 4.28: Dimensionless concentration vs A^* when $A = 0.2$, $Nb = Nt = 0.5$, $\gamma = 0.5$, $M = 2.5$, $Pr = 2$, $Le = 5$, $Bi = 5$, $\beta = 0.2$, $A^* = Gr = 0.1$, $B^* = 0.2$ and $Gc = 0.1$.

4.5.10 Temperature Dependent Heat Generation/Absorption Coefficient

Figure 4.29 depicts that by increasing the value of the temperature dependent heat generation/absorption coefficient B^*, velocity profile is increased. Figure 4.30 indicates the impact of the temperature dependent heat generation/absorption B^* on the temperature profile. This figure describes that by increasing the temperature dependent heat generation/absorption B^*, temperature profile increases. It is seen from Figure 4.31 that by increasing the value of the temperature dependent heat generation/absorption, the concentration profile shows an interesting behaviour. Initially, near the wall it increases, then decreases a bit away from the wall and again it starts increasing a bit further away from the wall.

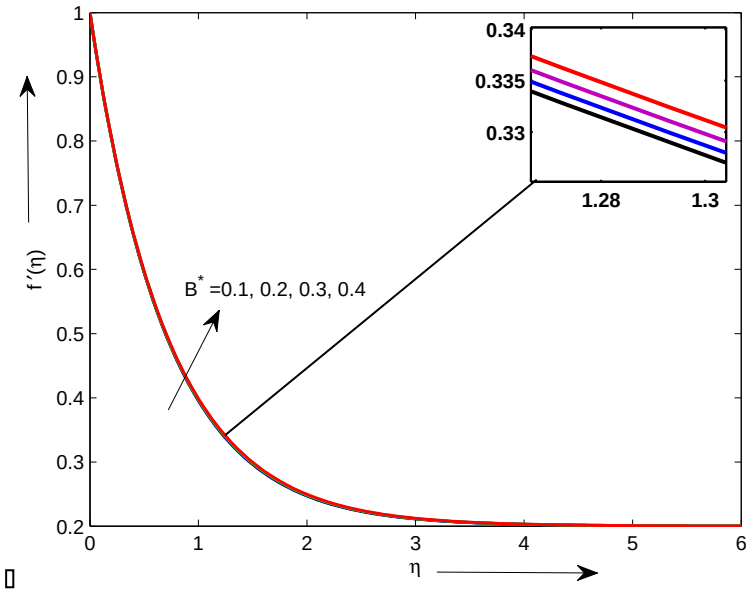

FIGURE 4.29: Dimensionless velocity vs B^* when $A = 0.2$, $Nb = Nt = 0.5$, $\gamma = 0.5$, $M = 2.5$, $Pr = 2$, $Le = 5$, $Bi = 5$, $\beta = 0.2$, $A^* = Gr = 0.1$, $B^* = 0.2$ and $Gc = 0.1$.

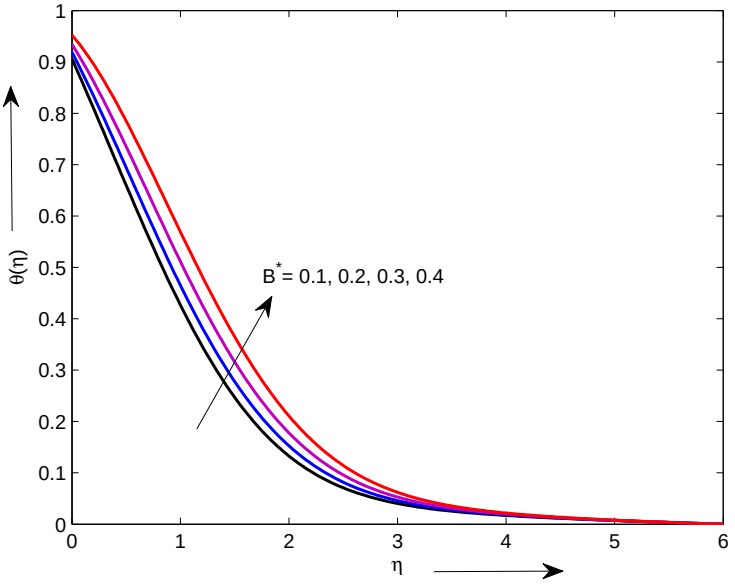

FIGURE 4.30: Dimensionless temperature vs B^* when $A = 0.2$, $Nb = Nt = 0.5$, $\gamma = 0.5$, $M = 2.5$, $Pr = 2$, $Le = 5$, $Bi = 5$, $\beta = 0.2$, $A^* = Gr = 0.1$, $B^* = 0.2$ and $Gc = 0.1$.

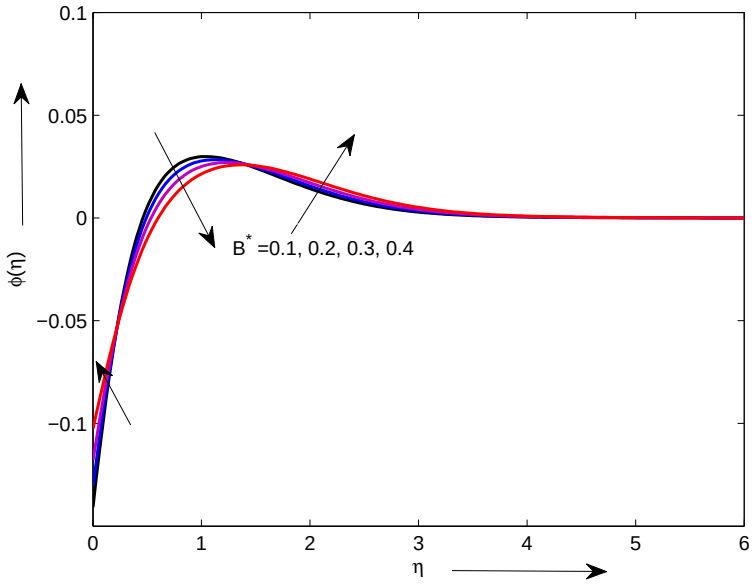

FIGURE 4.31: Dimensionless concentration vs B^* when $A = 0.2$, $Nb = Nt = 0.5$, $\gamma = 0.5$, $M = 2.5$, $Pr = 2$, $Le = 5$, $Bi = 5$, $\beta = 0.2$, $A^* = Gr = 0.1$, $B^* = 0.2$ and $Gc = 0.1$.

4.5.11 Chemical Reaction Parameter

Figure 4.32 shows that by increasing the chemical reaction parameter, the velocity profile decreases. Figure 4.33 illustrates the impact of the chemical reaction on the temperature profile for different values. It increases by increasing the value of the chemical reaction parameter γ. Effect of γ on the concentration is included in Figure 4.34. The concentration distribution increases with the increasing values of γ but a bit away from the surface it starts decreasing.

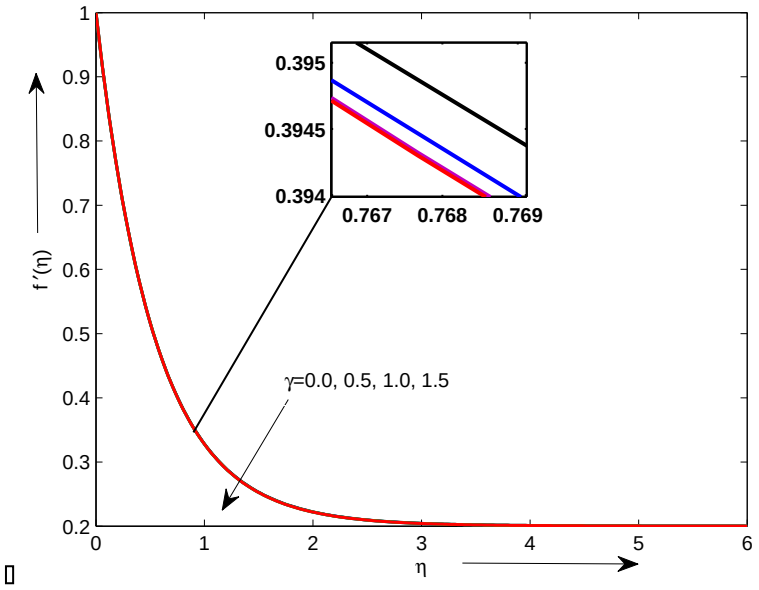

FIGURE 4.32: Dimensionless velocity vs γ when $A = 0.2$, $Nb = Nt = 0.5$, $\gamma = 0.5$, $M = 2.5$, $Pr = 2$, $Le = 5$, $Bi = 5$, $\beta = 0.2$, $A^* = Gr = 0.1$, $B^* = 0.2$ and $Gc = 0.1$.

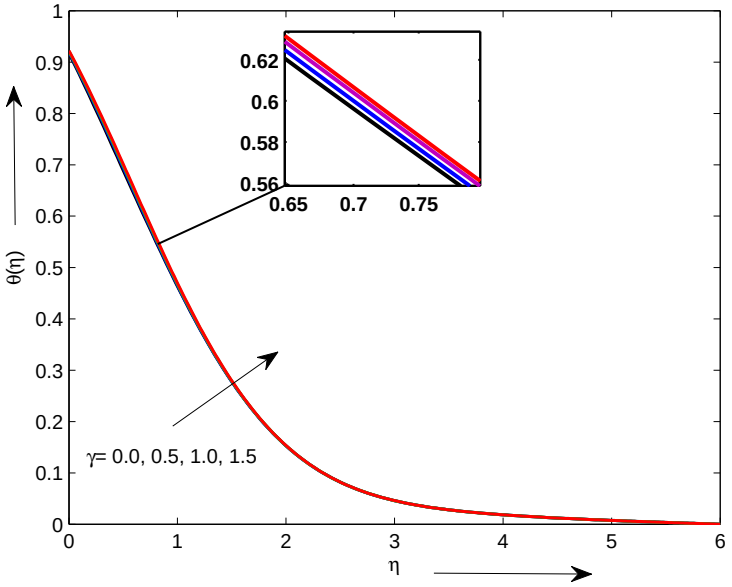

FIGURE 4.33: Dimensionless temperature vs γ when $A = 0.2$, $Nb = Nt = 0.5$, $\gamma = 0.5$, $M = 2.5$, $Pr = 2$, $Le = 5$, $Bi = 5$, $\beta = 0.2$, $A^* = Gr = 0.1$, $B^* = 0.2$ and $Gc = 0.1$.

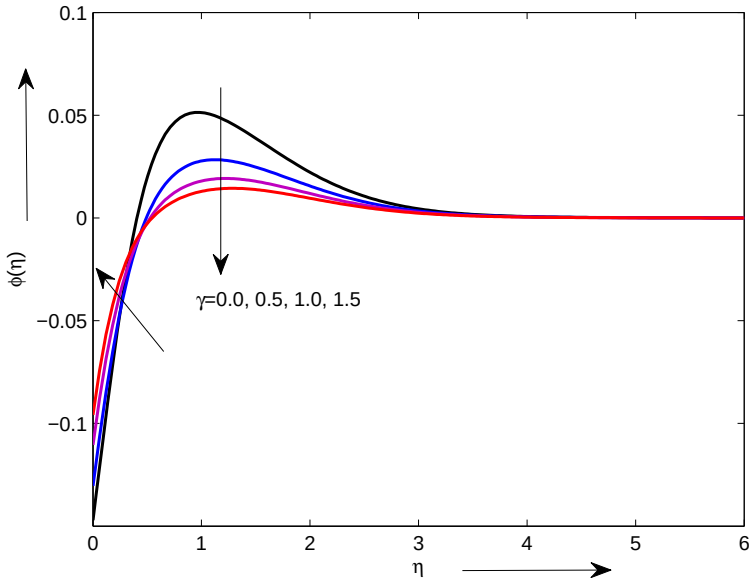

FIGURE 4.34: Dimensionless concentration vs γ when $A = 0.2$, $Nb = Nt = 0.5$, $\gamma = 0.5$, $M = 2.5$, $Pr = 2$, $Le = 5$, $Bi = 5$, $\beta = 0.2$, $A^* = Gr = 0.1$, $B^* = 0.2$ and $Gc = 0.1$.

4.5.12 Solutal Grashof Number

The effect of the solutal Grashof number on the velocity profile is presented in Figure 4.35. Increasing the solutal Grashof number Gc, the velocity profile is observed to increase. In case of the dimensionless temperature, the solutal Grashof number shows exactly the opposite behaviour, which can be seen through Figure 4.36. Figure 4.37 delineates that by increasing the solutal Grashof number, initially, the concentration profile decreases near the surface. It increases a bit away from the surface and then again it starts decreasing a bit further away from the surface.

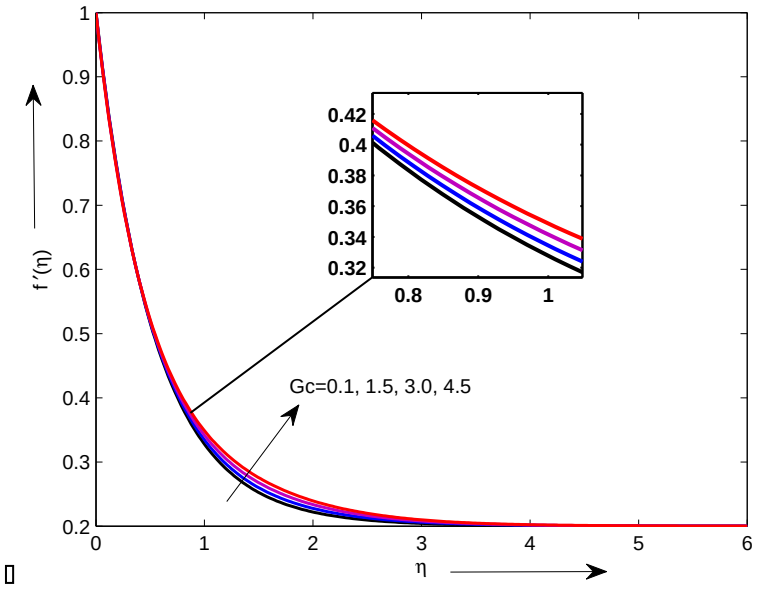

FIGURE 4.35: Dimensionless velocity vs Gc when $A = 0.2$, $Nb = Nt = 0.5$, $\gamma = 0.5$, $M = 2.5$, $Pr = 2$, $Le = 5$, $Bi = 5$, $\beta = 0.2$, $A^* = Gr = 0.1$, $B^* = 0.2$ and $Gc = 0.1$.

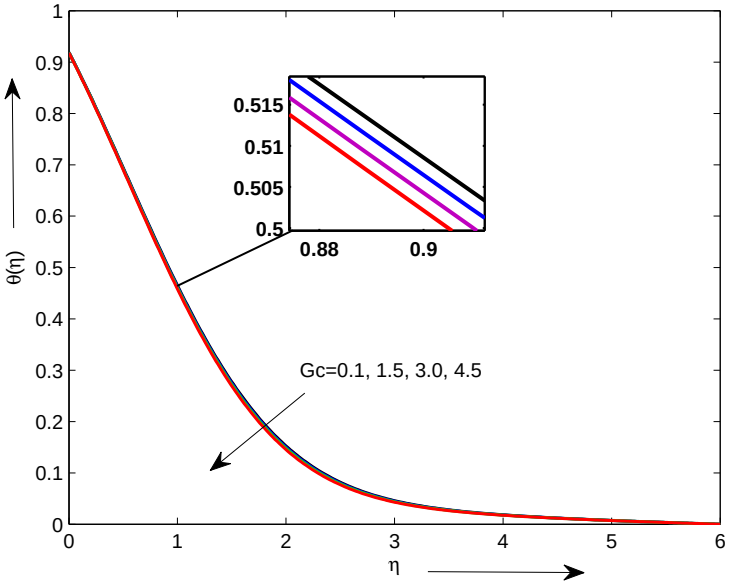

FIGURE 4.36: Dimensionless temperature vs Gc when $A = 0.2$, $Nb = Nt = 0.5$, $\gamma = 0.5$, $M = 2.5$, $Pr = 2$, $Le = 5$, $Bi = 5$, $\beta = 0.2$, $A^* = Gr = 0.1$, $B^* = 0.2$and $Gc = 0.1$.

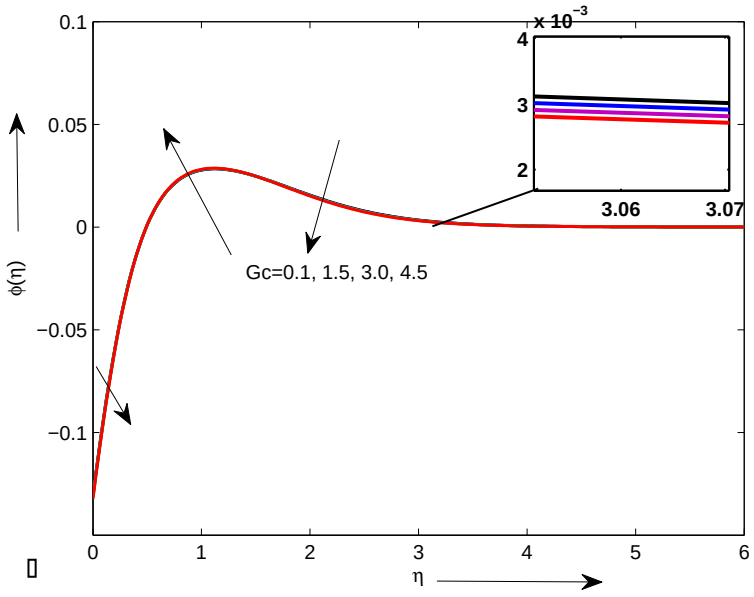

FIGURE 4.37: Dimensionless concentration vs Gc when $A = 0.2$, $Nb = Nt = 0.5$, $\gamma = 0.5$, $M = 2.5$, $Pr = 2$, $Le = 5$, $Bi = 5$, $\beta = 0.2$, $A^* = Gr = 0.1$, $B^* = 0.2$ and $Gc = 0.1$.

4.5.13 Thermal Grashof Number

The effect of the Gr on the velocity profile is shown in Figure 4.38. It is noticed that the thermal Grashof number contributes to increase the velocity profile if all other parameters that appear in the velocity field are kept constant. Figure 4.39 designates that by increasing the value of the thermal Grashof number, the temperature profile decreases. In Figure 4.40, the concentration profile shows an interesting behaviour for different values of the thermal Grashof number. Figure delineates that by increasing the thermal Grashof number, initially, the concentration profile decreases near the wall. It increases a bit away from the wall and then again it starts decreasing a bit further away from the wall.

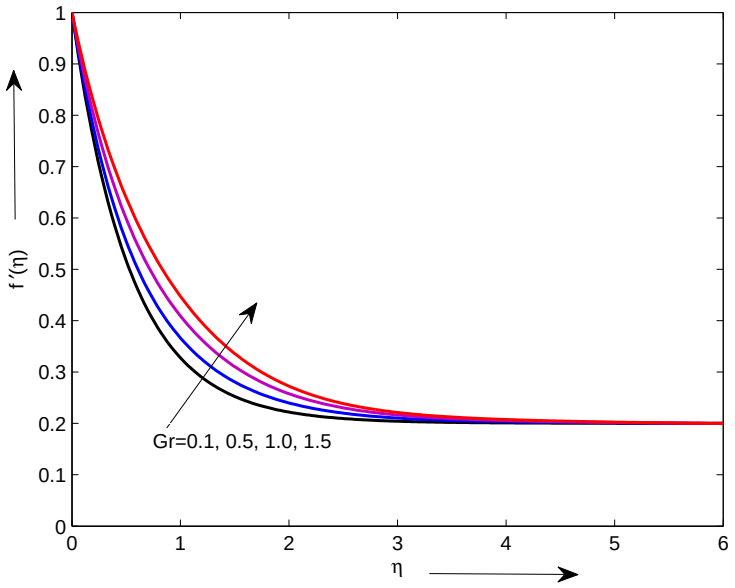

FIGURE 4.38: Dimensionless velocity vs Gr when $A = 0.2$, $Nb = Nt = 0.5$, $\gamma = 0.5$, $M = 2.5$, $Pr = 2$, $Le = 5$, $Bi = 5$, $\beta = 0.2$, $A^* = Gr = 0.1$, $B^* = 0.2$ and $Gc = 0.1$.

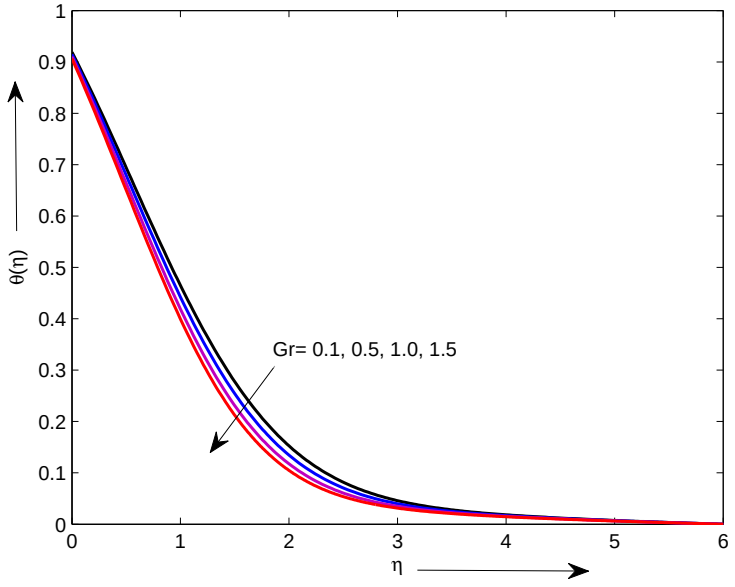

FIGURE 4.39: Dimensionless temperature vs Gr when $A = 0.2$, $Nb = Nt = 0.5$, $\gamma = 0.5$, $M = 2.5$, $Pr = 2$, $Le = 5$, $Bi = 5$, $\beta = 0.2$, $A^* = Gr = 0.1$, $B^* = 0.2$ and $Gc = 0.1$.

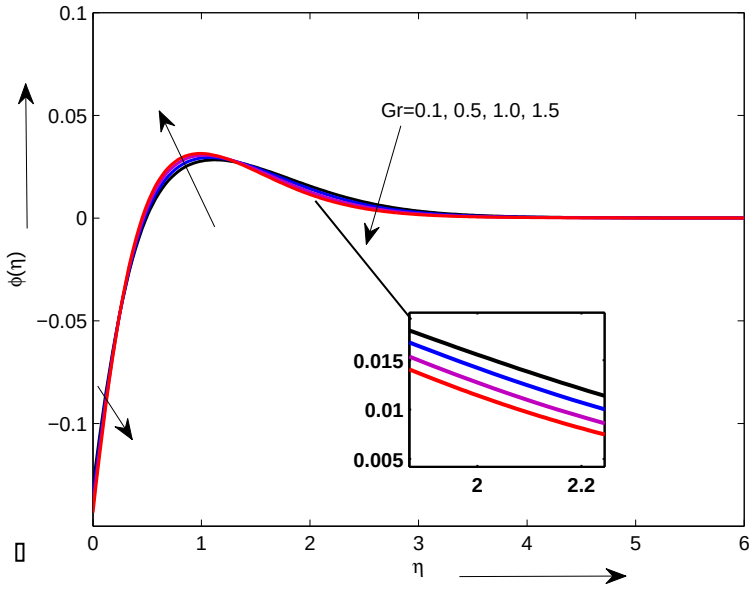

FIGURE 4.40: Dimensionless concentration vs Gr when $A = 0.2$, $Nb = Nt = 0.5$, $\gamma = 0.5$, $M = 2.5$, $Pr = 2$, $Le = 5$, $Bi = 5$, $\beta = 0.2$, $A^* = Gr = 0.1$, $B^* = 0.2$ and $Gc = 0.1$.

Chapter 5

CONCLUSION

In this thesis, a numerical study of chemical reaction and non-uniform internal heat source effects on MHD mixed convection stagnation point flow of Maxwell nanofluid over a stretching surface, is presented. The two-dimensional viscous flow of the nanofluid along with the convactive boundary conditions, was considered. Numerical solution of the mathematical model was carried out by using the shooting technique. A numerical comparison is exhibited with the Matlab built-in code bvp4c for various physical parameters affecting the flow and heat transfer and the results are found to be in a very good agreement. Significance of the effects of different physical parameters under discussion on the dimensionless velocity, temperature and concentration are delineated graphically. The skin friction coefficient and the Nusselt number for different value of the distinctive governing parameters are presented in the tabular form. After a thorough investigation, we have reached the following concluding observation.

- The velocity profile increases by increasing A but the temperature and concentration profiles decrease by increasing A.
- The magnetic parameter M has the same increasing influence on the temperature and the concentration field but opposite on the velocity field.
- The velocity field f', the temperature field θ and the concentration field ϕ reduce with an increase in the Prandtl number.
- The temperature field θ and the concentration field ϕ increase but the velocity field reduces by increasing Nb but Gc have exactly the opposite influence.

- The velocity field f' and the temperature field θ increase by increasing the value of Nt and Bi, but concentration field ϕ decreases for both the parameters.
- The Lewis number Le has an increasing effect on the velocity field f', temperature field θ and concentration field ϕ.
- The visco-elastic parameter β has an increasing effect on the velocity profile but decreasing on the temperature and concentration profiles.
- The space dependent heat generation/absorption coefficient A^* and the temperature dependent heat generation/absorption coefficient B^* have an increasing effect on the velocity field f', temperature field θ and concentration field ϕ.
- The temperature and concentration fields increase by enlarging the chemical reaction parameter γ but the velocity field decreases.
- The velocity f' and the concentration field ϕ increase by enhancing the solutal-Grashof number Gc and thermal Grashof number Gr but it cause a decrease in the temperature field.

Bibliography

[1] S. U. S. Choi. Enhancing thermal conductivity of fluids with nanoparticles. *ASME-Publications-Fed*, 231:99–106, 1995.

[2] J. Buongiorno. Convective transport in nanofluids. *Journal of Heat Transfer*, 128 (3):240–250, 2006.

[3] A. V. Kuznetsov and D. A. Nield. Natural convective boundary-layer flow of a nanofluid past a vertical plate. *International Journal of Thermal Sciences*, 49(2): 243–247, 2010.

[4] W. A. Khan and I. Pop. Flow and heat transfer over a continuously moving flat plate in a porous medium. *Journal of Heat Transfer*, 133(5):054501, 2011.

[5] L. Zheng, C. Zhang, X. Zhang, and J. Zhang. Flow and radiation heat transfer of a nanofluid over a stretching sheet with velocity slip and temperature jump in porous medium. *Journal of the Franklin Institute*, 350(5):990–1007, 2013.

[6] H. S. Takhar, R. S. R. Gorla, and V. M. Soundalgekar. Short communication radiation effects on MHD free convection flow of a gas past a semiinfinite vertical plate. *International Journal of Numerical Methods for Heat & Fluid Flow*, 6(2): 77–83, 1996.

[7] A. Y. Ghaly and M. E. E. Elsayed. Radiation effect on MHD free-convection flow of a gas at a stretching surface with a uniform free stream. *Journal of Applied Mathematics*, 2(2):93–103, 2002.

[8] S. P. A. Devi and M. Kayalvizhi. Analytical solution of MHD flow with radiation over a stretching sheet embedded in a porous medium. *International Journal of Applied Mathematics and Mechanics*, 6(7):82–106, 2010.

[9] O. D. Makinde, W. A. Khan, and Z. H. Khan. Buoyancy effects on MHD stagnation point flow and heat transfer of a nanofluid past a convectively heated stretching/shrinking sheet. *International Journal of Heat and Mass Transfer*, 62:526–533, 2013.

[10] H. I. Andersson. MHD flow of a viscoelastic fluid past a stretching surface. *Acta Mechanica*, 95(1):227–230, 1992.

[11] M. I. Char. Heat and mass transfer in a hydromagnetic flow of the viscoelastic fluid over a stretching sheet. *Journal of Mathematical Analysis and Applications*, 186(3): 674–689, 1994.

[12] H. Markovitz and B. D. Coleman. Incompressible second-order fluids. *Advances in Applied Mechanics*, 8:69–101, 1964.

[13] K. R. Rajagopal. A note on unsteady unidirectional flows of a non-newtonian fluid. *International Journal of Non-Linear Mechanics*, 17(5-6):369–373, 1982.

[14] K. R. Rajagopal and A. S. Gupta. An exact solution for the flow of a non-newtonian fluid past an infinite porous plate. *Meccanica*, 19(2):158–160, 1984.

[15] A. M. Siddiqui, P. N. Kaloni, and O. P. Chandna. Hodograph transformation methods in non-Newtonian fluids. *Journal of Engineering Mathematics*, 19(3):203–216, 1985.

[16] A. M. Siddiqui and P. N. Kaloni. Certain inverse solutions of a non-newtonian fluid. *International Journal of Non-linear Mechanics*, 21(6):459–473, 1986.

[17] O. P. Chandna and P. V. Nguyen. Hodograph method in non-Newtonian MHD transverse fluid flows. *Journal of Engineering Mathematics*, 23(2):119–139, 1989.

[18] P. V. Nguyen and O. P. Chandna. Non-Newtonian MHD orthogonal steady plane fluid flows. *International Journal of Engineering Science*, 30(4):443–453, 1992.

[19] R. Cortell. Heat transfer in a fluid through a porous medium over a permeable stretching surface with thermal radiation and variable thermal conductivity. *The Canadian Journal of Chemical Engineering*, 90(5):1347–1355, 2012.

[20] M. I. Khan, T. Hayat, M. Waqas, M. I. Khan, and A. Alsaedi. Impact of heat generation/absorption and homogeneous-heterogeneous reactions on flow of Maxwell fluid. *J. Mol. Liq.*, 233:465–470, 2017.

[21] M. I. Khan, T. Hayat, M. Waqas, and A. Alsaedi. Outcome for chemically reactive aspect in flow of tangent hyperbolic material. *J. Mol. Liq.*, 230:143–151, 2017.

[22] T. Hayat, M. Zubair, M. Waqas, A. Alsaedi, and M. Ayub. Impact of variable thermal conductivity in doubly stratified chemically reactive flow subject to non-Fourier heat flux theory. *J. Mol. Liq.*, 234:444–451, 2017.

[23] T. Hayat, M. Waqas, A. Alsaedi, G. Bashir, and F. Alzahrani. Magnetohydrodynamic (MHD) stretched flow of tangent hyperbolic nanoliquid with variable thickness. *J. Mol. Liq.*, 229:178–184, 2017.

[24] M. Waqas, T. Hayat, M.Farooq, S. A. Shehzad, and A. Alsaedi. Cattaneo-Christov heat flux model for flow of variable thermal conductivity generalized Burgers fluid. *J. Mol. Liq.*, 220:642–648, 2016.

[25] T. Hayat, M. Waqas, M. I. Khan, and A. Alsaedi. Impacts of constructive and destructive chemical reactions in magnetohydrodynamic (MHD) flow of Jeffrey liquid due to nonlinear radially stretched surface. *J. Mol. Liq.*, 225:302–310, 2017.

[26] T. Hayat, M. Waqas, S. A. Shehzad, and A. Alsaedi. Chemically reactive flow of third grade fluid by an exponentially convected stretching sheet. *J. Mol. Liq.*, 223: 853–860, 2016.

[27] T. Hayat, M.Waqas, S. A. Shehzad, and A. Alsaedi. A model of solar radiation and Joule heating in magnetohydrodynamic (MHD) convectiveflow of thixotropic nanofluid. *J. Mol. Liq.*, 215:704–710, 2016.

[28] T. Hayat, M. I. Khan, M. Waqas, A. Alsaedi, and T. Yasmeen. Diffusion of chemically reactive species in third grade fluid flow over an exponentially stretching sheet considering magnetic field effects. *Chin. J. Chem. Eng.*, 25:257–263, 2017.

[29] T. Hayat, M. Zubair, M. Waqas, A. Alsaedi, and M. Ayub. Application of non-Fourier heat flux theory in thermally stratified flow of second grade liquid with variable properties. *Chin. J. Phys.*, 55:230–241, 2017.

[30] M. Waqas, M. Farooq, M. I. Khan, A. Alsaedi, T. Hayat, and T. Yasmeen. Magnetohydrodynamic (MHD) mixed convection flow of micropolar liquid due to nonlinear stretched sheet with convective condition. *Int. J. Heat Mass Trans.*, 102:766–772, 2016.

[31] T. Hayat, M. I. Khan, M. Waqas, and A. Alsaedi. Mathematical modeling of non-Newtonian fluid with chemical aspects: Anew formulation and results by numerical technique. *Coll. Sur. A: Phys. Eng. Asp.*, 518:263–272, 2017.

[32] A. Alsaedi, M. Awais, and T. Hayat. Effects of heat generation/absorption on stagnation point flow of nanofluid over a surface with convective boundary conditions. *Commun. Nonlinear. Sci. Numer. Simulat.*, 17:42104223, 2012.

[33] T. Hayat, M. Awais, M. Qasim, and Awatif A. Hendi. Effects of mass transfer on the stagnation point flow of an upper-convected Maxwell (UCM) fluid. *Int. J. Heat Mass Trans.*, 54:37773782, 2011.

[34] T. Hayat, M. Mustafa, S. A. Shehzad, and S. Obaidat. Melting heat transfer in the stagnation-point flow of an upper-convected Maxwell (UCM) fluid past a stretching sheet. *Int. J. Numer. Meth. Fluids*, 68:233243, 2012.

[35] T. Hayat, M. Zubair, M. Waqas, A. Alsaedi, and M. Ayub. On doubly stratified chemically reactive flow of PowellEyring liquid subject to non-Fourier heat flux theory. *Res. Phys.*, 7:99–106, 2017.

[36] T. Hayat, M. Zubair, M. Waqas, A. Alsaedi, and M. Ayub. Impact of variable thermal conductivity in doubly stratified chemically reactive flow subject to non-Fourier heat flux theory. *J. Mol. Liq.*, 234:444–451, 2017.

[37] M. Waqas, T. Hayat, M.Farooq, S. A. Shehzad, and A. Alsaedi. Cattaneo-Christov heat flux model for flow of variable thermal conductivity generalized Burgers fluid. *J. Mol. Liq.*, 220:642–648, 2016.

[38] T. Hayat, M. Zubair, M. Waqas, A. Alsaedi, and M. Ayub. Application of non-Fourier heat flux theory in thermally stratified flow of second grade liquid with variable properties. *Chin. J. Phys.*, 55:230–241, 2017.

[39] T. Hayat, M. I. Khan, M. Waqas, A. Alsaedi, and M. Farooq. Numerical simulation for melting heat transfer and radiation effects in stagnation point flow of carbon-water nanofluid. *Comp. Methods Appl. Mech. Eng.*, 315:1011–1024, 2017.

[40] T. Hayat, M. I. Khan, M. Waqas, and A. Alsaedi. Effectiveness of magnetic nanoparticles in radiative flow of Eyring-Powell fluid. *J. Mol. Liq.*, 231:126–133, 2017.

[41] T. Hayat, M. Waqas, A. Alsaedi, G. Bashir, and F. Alzahrani. Magnetohydrodynamic (MHD) stretched flow of tangent hyperbolic nanoliquid with variable thickness. *J. Mol. Liq.*, 229:178–184, 2017.

[42] T. Hayat, M. Waqas, M. I. Khan, and A. Alsaedi. Impacts of constructive and destructive chemical reactions in magnetohydrodynamic (MHD) flow of Jeffrey liquid due to nonlinear radially stretched surface. *J. Mol. Liq.*, 225:302–310, 2017.

[43] T. Hayat, M. Waqas, S. A. Shehzad, and A. Alsaedi. Chemically reactive flow of third grade fluid by an exponentially convected stretching sheet. *J. Mol. Liq.*, 223: 853–860, 2016.

[44] T. Hayat, M. I. Khan, M. Waqas, and A. Alsaedi. Mathematical modeling of non-Newtonian fluid with chemical aspects: A new formulation and results by numerical technique. *Coll. Sur. A: Phys. Eng. Asp.*, 518:263–272, 2017.

[45] P. M. Krishna, S. Naramgari, and S. Vangala. Aligned magnetic field, radiation, and rotation effects on unsteady hydromagnetic free convection flow past an impulsively moving vertical plate in a porous medium. *International Journal of Engineering Mathematics*, 2014, 2014.

[46] M. A. Mansour, N. F. El-Anssary, and A. M. Aly. Effects of chemical reaction and thermal stratification on MHD free convective heat and mass transfer over a vertical stretching surface embedded in a porous media considering soret and dufour numbers. *Chemical Engineering Journal*, 145(2):340–345, 2008.

[47] S. Naramgari and C. Sulochana. Dual solutions of radiative MHD nanofluid flow over an exponentially stretching sheet with heat generation/absorption. *Applied Nanoscience*, 6(1):131–139, 2016.

[48] Ahmed A. Afify. MHD free convective flow and mass transfer over a stretching sheet with chemical reaction. *Heat and Mass Transfer*, 40(6-7):495–500, 2004.

[49] O. Anwar Bég, M. D. S. Khan, I. Karim, M. D. M. Alam, and M. Ferdows. Explicit numerical study of unsteady hydromagnetic mixed convective nanofluid flow from an exponentially stretching sheet in porous media. *Applied Nanoscience*, 4(8):943–957, 2014.

[50] S. Nadeem and R. U. Haq. Effect of thermal radiation for megnetohydrodynamic boundary layer flow of a nanofluid past a stretching sheet with convective boundary conditions. *Journal of Computational and Theoretical Nanoscience*, 11(1):32–40, 2014.

[51] W. Ibrahim and R. U. Haq. Magnetohydrodynamic (MHD) stagnation point flow of nanofluid past a stretching sheet with convective boundary condition. *Journal of the Brazilian Society of Mechanical Sciences and Engineering*, 38(4):1155–1164, 2016.

[52] M. Massoud. Engineering thermofluids : Thermodynamics, fluid mechanics, and heat transfer. 2005.

[53] T. R. Mahapatra and A. S. Gupta. Heat transfer in stagnation-point flow towards a stretching sheet. *Heat and Mass Transfer*, 38(6):517–521, 2002.

[54] A. Ishak, R. Nazar, and I. Pop. Mixed convection boundary layers in the stagnation-point flow toward a stretching vertical sheet. *Meccanica*, 41(5):509–518, 2006.

[55] M. M. Mahantesh W. Ibrahim, B. Shankar. Mhd stagnation point flow and heat transfer due to nanofluid towards a stretching sheet. *Int J Heat Mass Transf*, 56: 1–9, 2013.

[56] T. Hayat, M. Mustafa, S. A. Shehzad, and S. Obaidat. Melting heat transfer in the stagnation-point flow of an upper-convected maxwell (UCM) fluid past a stretching sheet. *International Journal for Numerical Methods in Fluids*, 68(2):233–243, 2012.